



[Click here to view linked References](#)

1
2 **Effects of Si Solution on Stability of Early 3d Transition-Metal Tri-**
3 **Aluminides, Al₃T (T = Sc, Ti and V)**
4
5

6
7 C. M. Fang*, Z. P. Que and Z. Fan
8

9 Brunel Centre for Advanced Solidification Technology (BCAST), Brunel University London,
10 Uxbridge, Middlesex UB8 3Ph, UK
11
12

13
14 * Corresponding author, e-mail: changming.fang@brunel.ac.uk
15
16
17
18
19
20
21
22
23
24
25
26
27
28
29
30
31
32
33
34
35
36
37
38
39
40
41
42
43
44
45
46
47
48
49
50
51
52
53
54
55
56
57
58
59
60
61
62
63
64
65

1
2
3
4 **Abstract**

5 Addition of the early 3d transition-metals results in formation of primary Al_3T (T = Sc, Ti and V) phases in
6 Al alloys during casting. The newly formed Al_3T particles not only improve the mechanical performance of the
7 products, but also act as grain-refiners in the solidification processes. Meanwhile, experiments found impacts of
8 impurities, such as Si on the formation of the Al_3T phases, which mechanism is not fully understood. We here
9 investigate effects of Si solution on the stability and crystal chemistry of the Al_3T phases using first-principles
10 density-functional theory. The study has revealed a rich variety of effects of Si solution on the Al_3T phases. Si
11 solution stabilizes the $\text{D0}_{22}\text{-Al}_3\text{Ti}$ structure so that it becomes the ground-state, taking over the binary $\text{D0}_{23}\text{-}$
12 phase. Si solution in $\text{D0}_{22}\text{-V}$ occurs only at elevated temperature. Si solution has little impact on the Al_3Sc phase
13 relationship. The obtained information helps characterize the $(\text{Al,Si})_3\text{T}$ particles in Al products, understand their
14 role in solidification and further design new Al alloys of desirable properties.
15
16

17
18 **Key words:** Aluminium; Si solution; transition metal tri-aluminites; phase relations; density functional theory.
19
20
21
22
23
24
25
26
27
28
29
30
31
32
33
34
35
36
37
38
39
40
41
42
43
44
45
46
47
48
49
50
51
52
53
54
55
56
57
58
59
60
61
62
63
64
65

1. Introduction

Addition of transition metals can improve the mechanical performance and corrosion resistance of Al alloys [1,2]. The early 3d transition metals have relatively low mass densities (3.0 g/cm³ for Sc, 4.5 g/cm³ for Ti and 6.1 g/cm³ for V) which are comparable to that of Al (2.7 g/cm³) [1,3]. This unusual character benefits manufacturing light-metal alloys of relatively small weight/volume ratios. The added early 3d transition metals during casting react with Al, forming Al₃T particles [4-7]. The newly formed micro-/nano-scaled Al₃T particles cause the improvement of the mechanic performance and chemical properties of the products for aerospace and automotive transport applications [7-12].

Those native Al₃T particles may act as potential grain-refiners during solidification of the Al alloys, as well [13-17]. The small lattice mismatch between the cubic L1₂-Al₃Sc [8] and α-Al [3] means high nucleation potency of L1₂-Al₃Sc substrates. Al₃Ti particles have been considered to act as a grain-refiner separately [18,19] or to work together with TiB₂ particles in the widely used Al-nTi-B ($n = 3, 5$) master alloys [20-22]. Native Al₃V particles perform grain-refinement in the Al(V) alloy [16,17]. Moreover, the early 3d transition metal tri-aluminides may also be formed at the joints during welding, e.g. Al₃Ti at Ti-containing metals/Al joints [23]. Thus, it is vital to have a comprehensive understanding about the phase relations, crystal structure and physical properties for furthering development of Al alloys of desirable properties, particularly for the recycling Al scrap/waste parts which may contain various impurities [24,25].

There are three most-likely phases for the tri-aluminides, the cubic L1₂- and the tetragonal D0₂₂- and D0₂₃-Al₃T for T = Sc, Ti and V [26,27]. The terms 'Al₃T' and 'TA₃' are exchangeable in rest of the paper. Their structures are schematically drawn in Figure 1.

In the cubic L1₂-Al₃T structure (Figure 1a), each T atom has 12 Al nearest neighbors in cuboctahedral coordination. Each Al atom has also 12 neighbors (four T and eight Al) and is in square-planar coordination of T (Figure 1d).

In the tetragonal D0₂₂-phase, all atoms are still in the ideal positions, but the symmetry is broken (Figure 1b). The T atoms are in distorted cuboctahedral coordination of Al. There are two types of Al coordination by T. One third of the Al atoms positioned in the same planes with T (with the coordinate component, $z = 0.0$ and 0.5 in Figure 1b) are in square-planar coordination by T (Figure 1d). The rest (with $z = 0.25$ and 0.75) are tetrahedrally coordinated by T (Figure 1e).

In the D0₂₃-phase, not only the symmetry is broken but also the atomic positions deviate from the ideal sites. The local coordination thus, becomes distorted. All the T are still in distorted cuboctahedral coordination by Al. One third of the Al atoms ($z = 0.375$ and 0.875 in Figure 1c) are in the distorted tetrahedral coordination by T and the other two thirds are in distorted square-planar coordination with the Al being out of the T planes.

Overall, the L1₂, D0₂₂ and D0₂₃ structures (Figure 1) can be regarded as face-centred cubic (FCC) superstructures. The different coordination, broken symmetry and local structural distortion in the D0₂₂- and D0₂₃-phases would have impact on their stability and content of Si solution at the Al sites.

The phase relationships of the early 3d transition metal tri-aluminides have been a topic of intensive study both experimentally [4-7,26] and theoretically [27-29]. It is generally concurred that the ground state Al₃Sc has the cubic L1₂-type structure (Figure 1a) [4,8,10,28], and Al₃V the tetragonal D0₂₂-type structure [7,11,16,29].

There have been intensive discussions about the phase relations for Al₃Ti as summarized in [27]. The advanced first-principles investigations established that the D0₂₃-phase is the ground state for Al₃Ti [27,30]. Meanwhile, the experiments produced a scattering of results. The thermodynamics study for the binary Al-Ti phase diagrams suggested phase transition between a high-temperature phase to a low-temperature one with variable transition temperatures [5, 31,32]. Structural characterization revealed formation of D0₂₂-Al₃Ti particles in manufactured Al products [33-35]. Furthermore, the lattice parameters for the Al₃Ti phases in different samples vary notably [27,33-35]. The latter is also true for the observed D0₂₂- Al₃V samples [35,36].

Impurities including Si exist inevitably in commercial Al metals [37]. Si is often added into Al to obtain products of desirable properties for applications at extreme conditions, e.g. high temperatures [1,2]. Hence it is necessary to have a good understanding about Si solution in the early 3d transition-metal tri-aluminides and the corresponding effects on their stability and structural properties.

There have been efforts on Si solution in the Al₃T phases [38, 39] along with the intensive study on the binary phases [4-8,10,26-30, 40, 41]. Recently, Dumbre *et al.* studied the impact of thermal treatments on formation of (L1₂)-(Al,Si)₃Sc in Al-Si-Sc alloys [43]. Yao performed first-principles calculations on the elastic and electronic properties of L1₂-(Al,Si)₃Sc phase [44]. Using first-principles density functional theory approach, Castillo-Sánchez *et al.* investigated Si substitution in the Al₃(Zr,Ti) intermetallic compounds with the D0₂₂- and D0₂₃-type structures [39]. Meanwhile, there is still a lack of comprehensive understanding about the Si solution in the early 3d transition metal tri-aluminides phases.

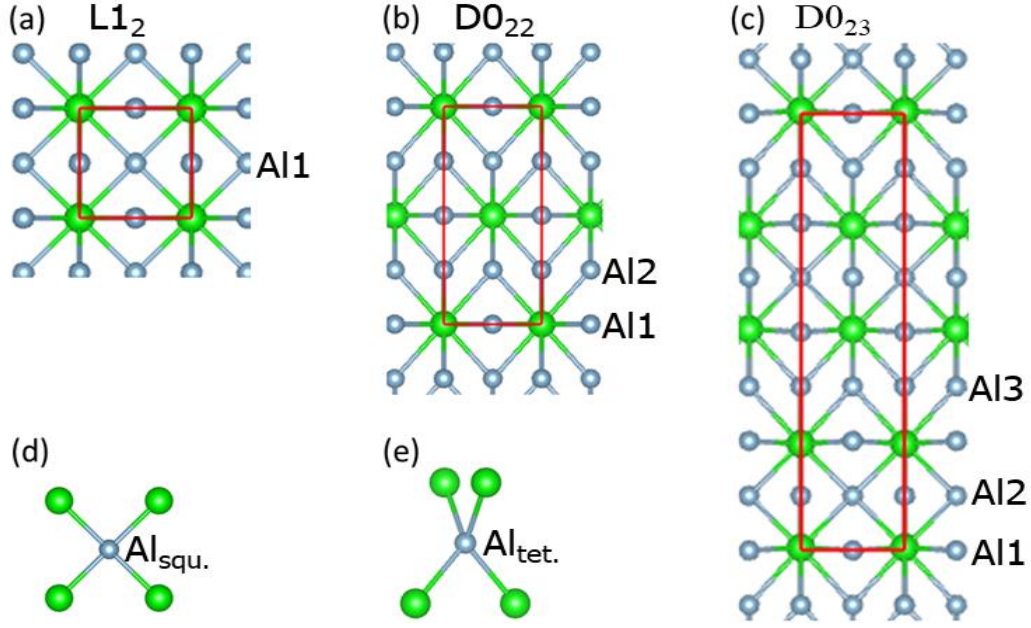


Figure 1. Schematic structures of the $L1_2$ - (a), $D0_{22}$ - (b) and $D0_{23}$ - TAl_3 (c) projected along the $[100]$ orientations, and local coordination of Al atom in a square-planar (d) and tetrahedral (e) coordination by four T atoms. The red-lines means the b -axis (horizontal) and c -axis (vertical) in (a), (b) and (c). The z -component of the unit cell for $D0_{23}$ - TAl_3 has been shifted by $1/8$, which sets the Al atoms at the Wyckoff 4e sites atoms at $z = 0$. The larger green spheres represent Ti and smaller silvery Al.

Here we investigate Si solution in the Al_3T ($T = Sc, Ti$ and V) forms of $L1_2$ -, $D0_{22}$ - and $D0_{23}$ -type structures in a systematic way using a first-principles density-functional theory method. This study reveals that Si solution favors the Al sites in Ti square-planar coordination (Figure 1d) and stabilizes the $D0_{22}$ - Al_3Ti phase so that the $D0_{22}$ - $(Al_{1-x}Si_x)_3Ti$ phases become more stable than the binary ground state ($D0_{23}$ - Al_3Ti) phase. The Si solution in $D0_{22}$ - Al_3V occurs only at elevated temperatures. The obtained information here helps not only understand the phase relationships and the rich variety of experimental results in the literature, but also design new Al alloys of desirable mechanical and chemical properties based on Al scrap/waste parts, which benefits develop our circular society in an environmental-friendly sustainable way.

2. Details of computations

To assess the relative stability of the binary Al_3T compounds, the energy difference between the investigated $X-Al_3T$ and the corresponding cubic $L1_2$ -phase is defined as:

$$\Delta E_1 = E(X-Al_3T) - E(L1_2-Al_3T) \quad (1)$$

Here, $E(X-Al_3T)$ and $E(L1_2-Al_3T)$ represent the calculated total valence-electron energies for the related X -phase and related $L1_2$ - Al_3T phase, respectively.

For dilute solution of Si and the early 3d transition metals in the Al matrix, the solution energy is defined as:

$$\Delta E(M^*) = E(Al_{n-1}M) - [(n-1)/n \times E(Al_n) + E(M)] \quad (2)$$

Where, $E(Al_{n-1}M)$, $E(Al_n)$, $E(M)$ represent respectively, the calculated energies for the substituted $Al_{n-1}M$, Al_n and the elemental solid M . The calculated total valence-electron energy of the same supercell of Al_n is used for systematic error cancellation. The unit of the solution energy is eV per M.

For a ternary Si doped $(Al_{1-x}Si_x)_3T$ phase, the formation energy with respect to the elemental solids Si, Al and dilute solution of T in the Al matrix is defined as,

$$\Delta E_f = E[(Al_{1-x}Si_x)_3T] - \{3(1-x)E(Al) + 3xE(Si) + E(T^*)\} \quad (3)$$

Here $E[(Al_{1-x}Si_x)_3T]$, $E(Al)$, $E(Si)$ and $E(T^*)$ represent the calculated total valence-electron energies for the $(Al_{1-x}Si_x)_3T$ phase, the elemental solids Al and Si, and the dilute solution of a 3d transition metal, T in the Al matrix (T^*) in Equation 2, respectively.

The unit for both Equations 1 and 3 is eV/f.u. (f.u. represents formula unit, $(Al_{1-x}Si_x)_3T$). A negative ΔE_1 value in Equation 1 means that the $X-Al_3T$ is more stable than the $L1_2$ -phase. For Equation 3, a negative value of the formation energy means favoring formation of the $(Al_{1-x}Si_x)_3T$ phase with respect to the elemental solids,

Al, Si and T*. At $T = 0$ K and $P = 0$ Pa, the calculated formation energy in Equations 2 and 3 is equal to the related reaction enthalpy when the zero-vibration contribution is ignored.

A $3a_0 \times 3a_0 \times 3a_0$ (a_0 is the lattice parameter of the cubic Al unit cell) supercell which contains 108 Al atoms is employed to model the dilute solution of Si and an early 3d transition metal in the Al matrix. $2a_0 \times 2a_0 \times 2a_0$ ($3a_0 \times 3a_0 \times 3a_0$), $2a_0 \times 2a_0 \times 1c_0$ and $2a_0 \times 2a_0 \times 1c_0$ (a_0 and a_0 are the lattice parameters of the conventional cells for the corresponding structures) supercells are used for the cubic L1₂-, tetragonal D0₂₂- and D0₂₃-Al₃T phases and they contain 32(108), 32, and 64 atoms, respectively. The large supercell $3a_0 \times 3a_0 \times 3a_0$ for the L1₂-phase was utilized to justify the usage of the smaller supercells.

A plane-wave approach embedded in the first-principles package VASP (Vienna *Ab initio* Simulation Package) [45] has been employed in the present study. The Generalized Gradient Approximation (GGA) [46] within the projector-augmented wave frame [47] has been used for the correlation and exchange terms. This is because that the GGA works better than the Local Density Approximations (LDA) for transition metals and their compounds [46,48,49]. Cut-off energies are reasonably high ($E_{\text{CUT}}/E_{\text{AUG}} = 400.0$ eV/550.0 eV) compared with the default values of the atoms ($E_{\text{MAX}}/E_{\text{AUG}} = 245.3$ eV/322.1 eV for Si, 180.2 eV/240.3 eV for Al, 116.1 eV/154.8 eV for Sc, 133.7 eV/178.3 eV for Ti, and 144.4 eV/192.5 eV for V, respectively). Dense k -meshes for the structural optimizations and total energy calculations are used, e.g. a $10 \times 10 \times 10$ mesh with k -points ranging from 35(75) to 250(500) for the L1₂- and (D0₂₂-)Al₃T supercells, and a $10 \times 10 \times 6$ mesh with k -points ranging from 45 to 300 for D0₂₃-Al₃T supercells, depending on the symmetry in the Brillouin Zone for the based on the Monkhorst-Pack scheme [50]. Test calculations for the cut-off energies and k -meshes provided that the present settings are reasonable with energy deviations being less than 1 meV/atom.

3. Results and Discussion

3.1. Calculated results for the elemental solids and dilute solutions

First, structural optimizations were performed for the elemental solids, α -Al with the face-centred cubic structure and Si with the diamond-type structure, as well as the early 3d transitions metals [3,26]. Both Sc and Ti have simple hexagonal lattices, while V has a body-centred cubic structure [3]. We also performed calculations for dilute solution of the early 3d transition metals in Al. The obtained results are listed in Table I. The available experimental data in the literature are included for comparison.

Table I. The calculated results (lattice parameters, formation energies and important interatomic distances) for the elemental solids, Al, Si, Sc, Ti and V, and the dilute solution of Si and the early 3d transition metals in the Al matrix. The solution energy, $\Delta E(M^*)$ is obtained according to Equation 2. The electronic configurations for the elements are listed in which the element labels in the square parenthesis represents the core electrons. $\Delta = (d_{\text{calc}} - d_{\text{exp}})/d_{\text{exp}} \times 100$ represents the deviations of the computed lattice parameters (d_{calc}) from the corresponding experimental values extended to 0 K (d_{exp}) in [3] in the parenthesis. BCC represents body-centred cubic.

Element /ele.config.	Symmetry	Latt. para. (Å) and (Δ) (exp. data at 0 K[3])	Interatomic Distances (Å) and coordination-type
Al [Ne]3s ² 3p ¹	Cubic Fm-3m (nr. 225)	$a = 4.039(0.2 \%)$ (4.0325)	Al-Al: 2.86($\times 12$) (cuboctahedral)
Si [Ne]3s ² 3p ²	Cubic Fd-3m (nr. 227)	$a = 5.468(+0.7 \%)$ (5.42982)	Si-Si: 2.37($\times 4$) (tetrahedral)
Sc [Ar]4s ² 4p ⁰ 3d ¹	Hexagonal P6 ₃ /mmc (nr. 194)	$a = 3.320(+0.5 \%)$ (3.3035) $c = 5.157(-1.9 \%)$ (5.2552)	Sc-Sc: 3.21($\times 6$), 3.32($\times 6$) (distorted anticuboctahedral)
Ti [Ar]4s ² 4p ⁰ 3d ²	Hexagonal P6 ₃ /mmc (nr. 194)	$a = 2.929(-0.5 \%)$ (2.9451) $c = 4.593(-1.8 \%)$ (4.6783)	Ti-Ti: 2.85($\times 6$), 2.93($\times 6$) (distorted anticuboctahedral)
V [Ar]4s ² 4p ⁰ 3d ³	BCC, Im-3m (nr. 229)	$a = 2.978(-1.5 \%)$ (3.0223)	V-V: 2.58($\times 8$) (cubic)
Dilute solution of impurities in Al matrix (see Equation 2)			
Al ₁₀₇ M	Local symmetry	$\Delta E(M^*)$	T-Al bonds (Å)
Sc*	O _h	-1.04 eV/Sc	Sc - Al: 2.90($\times 12$)
Ti*	O _h	-1.18 eV/Ti	Ti - Al: 2.83($\times 12$)
V*	O _h	-0.57 eV/V	V - Al: 2.78($\times 12$)
Si*	O _h	+0.43 eV/Si	Si -Al: 2.84($\times 12$)

The calculations reproduced the experimental values well for the simple s-p elements, Al and Si with deviations within 1 %. Meanwhile for the early 3d transition metals, the calculated lattice parameters deviate somewhat larger, 1.5 % for the cubic V and about 1.8 %/1.9 % for the c-axis of the hexagonal lattices for Sc/Ti, respectively from the experimental values in the literature [3]. The calculated local Al-T bond-lengths in the dilute solutions decreases with increasement of valence electrons in the order, Sc, Ti and V, which is in line with the atomic radii in the pure metals (Table I). The calculated solution energies for the early 3d transition metals in the Al matrix are negative, indicating solution in Al matrix are favored with respect to the elemental solids. Meanwhile, Si solution in Al is not favored with a notable formation energy of 0.43 eV/Si which agrees with the previous calculations using the same approach [37,48]. The calculated Si-Al interatomic distance is 2.84 Å, which is slightly shorter than that of the Al-Al bonds. This result indicates that Si prefers not dissolving in the Al lattice. Thus, the energy of bulk Si is used as a reference to assess the stability of the compounds in equilibrium.

3.2. Binary Al₃T phases

Structural optimizations and total-energy calculations were carried out for the binary Al₃T phases. We also calculated the formation energies for the related D0₁₉-Al₃T structure [26,27]. The calculations showed that the D0₁₉-Al₃T phases are notably less stable with the calculated energies being over 4.0 eV/f.u. higher than those of the corresponding L1₂-Phases. Thus, the results for the D0₁₉-Al₃T phases are not discussed in the present paper. The calculated results for the L1₂-, D0₂₂- and D0₂₃-phases are listed in Table II. The experimental values available in the literature are included in parenthesis for comparison.

Table II. The calculated results (lattice parameters, formation energies and intermetallic bonds) in the binary TAl₃ (T = Sc, Ti, V) phases. The energy difference, ΔE_I are obtained via Equation 1. The experimental lattice parameters available in the literature are included in parenthesis together with the references. The most stable phases are marked in **bold**.

Phase	Latt. / Spacegroup	Latt. paras (Å), vol.(Å ³ /f.u.), ΔE_I (eV/f.u.)			Remarks
		Al ₃ Sc	Al ₃ Ti	Al ₃ V	T are in Al cuboctahedral coordination.
L1 ₂	Cubic Pm-3m (nr. 221)	$a = 4.103$ (4.106[8]) (4.105[51]) $V = 69.20$ $\Delta E_I = \mathbf{0.0}$	$a = 3.977$ (3.967[50]) (-) $V = 62.91$ $\Delta E_I = 0.0$	$a = 3.897$ (-) (-) $V = 59.19$ $\Delta E_I = 0.0$	Al is coordinated in T square-planar coordination (Fig.1d).
D0 ₂₂	Tetragonal I4/mmm (nr. 139)	$a = 4.021$ (-) (-) $c = 8.805$ (-) (-) $V = 71.17$ $\Delta E_I = +0.364$	$a = 3.841$ (3.836 to 3.854 [27]) (3.849 [34]) $c = 8.618$ (8.584 to 8.612[27]*) (8.610[34]) $V = 63.57$ $\Delta E_I = -0.108$	$a = 3.765$ (3.722[36]) (3.779[52]) $c = 8.307$ (8.195[36])* (-) (8.322[52])* $V = 58.86$ $\Delta E_I = -0.541$	Two types of Al Al1 at 2b in T square-planar coordination (Fig.1d) Al2 at 4d in T tetrahedra coordination (Fig.1e) *The experimental D0 ₂₂ -Al ₃ Ti/Al ₃ V samples prepared with different chemical compositions.
D0 ₂₃	Tetragonal I4/mmm (nr. 139)	$a = 4.039$ (-) (-) $c = 17.218$ (-) (-) $V = 70.23$ $\Delta E_I = +0.184$	$a = 3.895$ (3.875 to 3.947[27]) $c = 16.662$ (16.679 to 16.926[27]*) $V = 63.19$ $\Delta E_I = -0.131$	$a = 3.806$ (-) (-) $c = 16.315$ (-) (-) $V = 59.08$ $\Delta E_I = -0.268$	There three types of Al Al1 at 4e and Al2 at 4c are in distorted square-planar coordination by T with Al out of the Ti plane. Al3 at 4d are in distorted tetrahedra coordination.

As shown in Table II, the present calculations produced the following results.

1). With increasing the number of d electrons in the transition metal, L1₂-Al₃Sc, D0₂₃-Al₃Ti and D0₂₂-Al₃V are the ground state phases. D0₂₃-Al₃Ti has a formation energy being 0.02 eV/f.u. lower than its D0₂₂-phase. This conclusion agrees with the previous works [27-29].

2). The calculated lattice parameter of L1₂-Al₃Sc is close to the experimental values from different groups [8,51]. Meanwhile, the experimental values for the ground state D0₂₂-Al₃V differ notably from each other [36,52]. The calculated lattice parameters are in-between those of the available experimental data (Table II).

3). As summarized in the references [27,52], the experimental lattice parameters for both $D0_{22}$ - and $D0_{23}$ - Al_3Ti phases in the literature vary in ranges within 2 %. The calculated values are close to the experimental values.

Intrinsic defects in the Al_3T phases have been investigated. There are high energy costs for Al substitutions of T in the ground state Al_3T phases ($L1_2$ - Al_3Sc , $D0_{23}$ - Al_3Ti and $D0_{22}$ - Al_3V). For example, it costs over 0.70 eV to replace one T by Al with respect to T solution in the Al matrix. The calculations also produced high energy costs to produce Al vacancies, e.g. it costs 0.81 eV to create one Al vacancy in the $L1_2$ - Al_3Ti phase. The calculations indicate unlikeliness for the intrinsic defects to occur. Therefore, we limit ourselves to Si dissolving at the Al sites in the compounds.

3.3 Effects of Si solution on stability of the Al_3T phases

The study includes various configurations of Si solution at the Al sites in the Al_3T phases. It showed that the Si atoms prefer uniform layer-resolved distributions in the structures. For example, for two Si doped at the Al1 sites in the $D0_{23}$ - Al_3Ti supercell there are four equal layers, $z = 0.0, \frac{1}{4}, \frac{1}{2}$ and $\frac{3}{4}$ (Figure 1c). The calculations showed that the formation energies for the configuration with two Si at the same layer ($z = 0.0$) and that with two Si at the nearby layers ($z = 0.0$ and 0.25) are, respectively about 0.04 eV and 0.02 eV higher than that with the Si atoms uniformly distributed (Si1 at $z = 0.0$ and Si2 at $z = 0.50$). This helps us choose configurations of high stability. The results for Si solution at the Al sites in the Al_3T phases are addressed separately in the following subsections.

3.3.1 Si solution in Al_3Sc

Figure 2 shows the calculated formation energies for the highly stable configurations with Si solution in the Al_3Sc phases. Clearly, Si solution in $L1_2$ - Al_3Sc cost a notable amount of energy. Doping one Si at the Al site costs 0.28 eV, indicating that it is highly unlikely to occur at low temperature. However, at high temperature, kinetic factor enables dope a moderate amount of Si at the Al sites, which agrees with experimental assumptions [43].

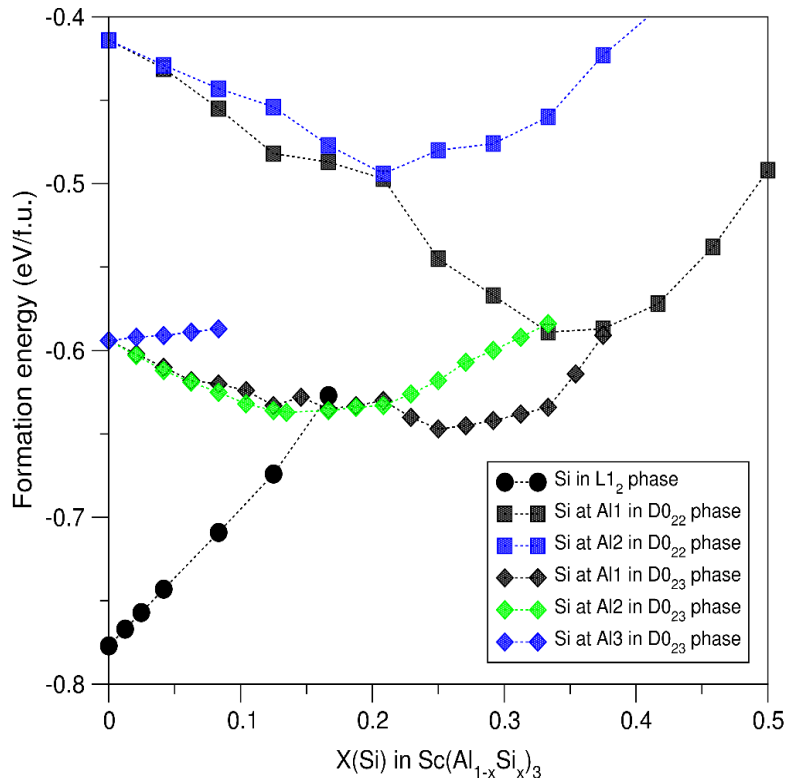


Figure 2. The dependences of the formation energies on Si content in the Al_3Sc phases. Clearly, the binary $L1_2$ - Al_3Sc is the most stable phase in the system.

Si solution at the Al sites in $D0_{22}$ - Al_3Sc phases is favored. With increasing Si content, the configurations become more stable. The most stable configuration is the full Si occupation of the Al1 site, which has the chemical formula, $D0_{22}$ - Al_2SiSc . This configuration gains a notable amount of energy (about 0.17 eV/f.u.).

However, such an energy gain is not enough to make this phase more stable than $L1_2$ - Al_3Sc . Addition of extra Si at the Al2 sites gradually reduces the stability of $D0_{22}$ - Al_2SiSc .

For the $D0_{23}$ -phase, Si prefers the Al1 and Al2 sites where Al atoms are in distorted Ti square-planar coordination, meanwhile Si solution at the Al3 sites with distorted Ti tetrahedral coordination costs moderate energies. The most stable configuration has the chemical formula, $D0_{23}$ - $(Al_{0.708}Si_{0.292})_3Sc$. This formation energy is still much higher than the binary cubic $L1_2$ -phase as shown in Figure 2.

Overall, the calculations revealed preference of Si solution in $D0_{22}$ - and $D0_{23}$ - Al_3Sc . The Si stabilization, however, is not strong enough to overtake the ground state $L1_2$ - Al_3Sc phase. This study elucidates the experimental observations that this cubic phase exists and has been observed in the Al alloys. Moreover, the measured lattice parameters of $L1_2$ - Al_3Sc in the Al alloys of different Si contents are close to each other [8,43,51], indicating minor Si content.

3.3.2. Si solution stabilizes $D0_{22}$ - Al_3Ti

The calculations revealed that Si solution in $L1_2$ - Al_3Ti is not favored with an energy cost of 0.43 eV to replace one Al by Si. Such energy cost is the close to that to dope one Si in bulk Al (Table I), indicating highly impossible to occur.

Doping one Si atom at both Al1 and Al2 sites costs 0.16 eV and at the Al3 sites 0.28 eV in the $D0_{23}$ -phase, respectively. The Si doping at the Al1 sites is shown in Figure 3. The formation energy increases almost linearly with the Si content in the $D0_{23}$ -phase.

Si solution at both Al1 and Al2 sites in $D0_{22}$ - Al_3Ti is favored. The formation energy for one Si at the Al1 sites is about 0.05 eV lower than that at the Al2 sites, indicating the former is preferred over the latter. The trends of relationships between the formation energies and Si content for Si solution at the Al1 and the Al2 sites are shown in Figure 3. The formation energy decreases with increase of Si content and reach minima at $x(Si) = 1/6$ in $(Al_{1-x}Si_x)_3Ti$. It then increases with further addition of Si. Thus, the most stable configurations have chemical composition, $D0_{22}$ - $(Al_{0.833}Si_{0.167})_3Ti$ with Si at Al1. Analysis showed that the most stable configuration of the composition, the Si atoms are distributed away from each other, in a uniform way. This Si content is notably lower than that in the reported $D0_{22}$ - $(Al_{2/3}Si_{1/3})_3Ti$ with the Si full occupation of the 2b (Al1) sites, which configuration has the minimum enthalpy in the Al_3Ti - Si_3Ti system in the recent publication (Figure 12 in [39]).

Figure 3 revealed that the formation energies for the configurations with over 2 at.% Si at the Al1 sites in the $D0_{22}$ -phase are lower than that of the ground state $D0_{23}$ - Al_3Ti phase. This indicates that the Si doped $D0_{22}$ -phase replaces the binary $D0_{23}$ - Al_3Ti phase to be the ground state.

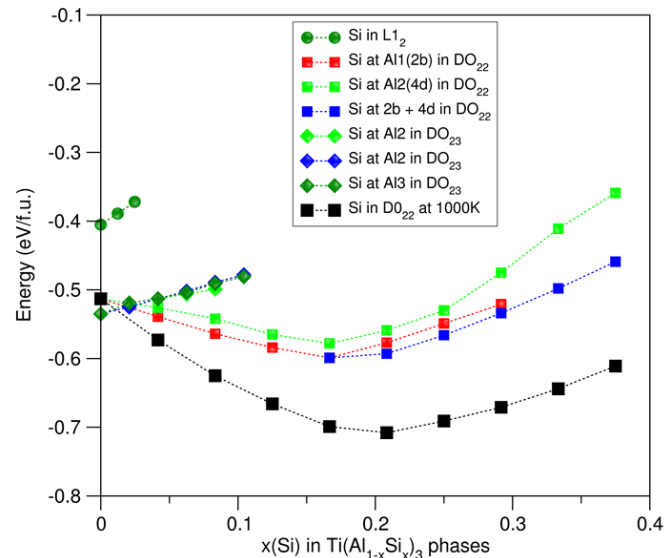


Figure 3. Relationships between the formation energies and Si content in the $(Al_{1-x}Si_x)_3Ti$ phases. Clearly, Si solution stabilizes the $D0_{22}$ -phase that it overtakes the $D0_{23}$ - Al_3Ti phase as the ground state.

The partial occupation of Si at the Al sites indicates the important role of configurational entropy contributions in the stability at elevated temperature. The stability of the Si doped $D0_{22}$ -phase at the casting temperature can be estimated via the Gibbs energy, $\Delta G = \Delta H - T\Delta S_{conf}$, where ΔH is the formation enthalpy being equal to ΔE_f at 0 K and 0 Pa, when the zero-point vibration contribution is ignored, T is the temperature, the configurational entropy, $\Delta S_{conf} = R \ln W$ (R is the Boltzmann constant and W the number of configurations in

the random model, considering kinetic factor over the moderate energy hierarchy ($<0.05\text{eV/f.u.}$) at such high temperature. The obtained values for the Gibbs energies at 1000 K are plotted in Figure 3.

Figure 3 shows a shallow potential valley for the Gibbs energy on Si in the range $x = 0.17$ to 0.25 in the formula $\text{D0}_{22}\text{-(Al}_{1-x}\text{Si}_x)_3\text{Ti}$ at the casting temperature with the minimum at $x = 0.208$. This indicates dependence of Si content in the obtained samples on the local chemical composition and thermal treatments.

In brief, Si solution is favored in $\text{D0}_{22}\text{-Al}_3\text{Ti}$. The partial occupation of Si at the Al sites also indicates dependence on the chemical composition and preparation conditions. With a moderate Si content (2 at%Si), the D0_{22} -phase overtakes the D0_{23} -phase as the ground phase. This study provides explanation about the long-standing puzzle that the Al_3Ti particles observed in most Al-alloys have the D0_{22} -type structure [33-35], whereas the theoretical calculations predicted that the $\text{D0}_{23}\text{-Al}_3\text{Ti}$ is the ground state in the Al-Ti system [27,30].

3.3.3. Si solution in Al_3V

Figure 4 shows the calculated relationships between the formation energies and Si contents at the Al sites in the Al_3V phases. There are rather simple relations between the formation energies and Si solution at the Al sites for the Al_3V phases that it costs energies for Si solution in any of the phases. Thus, there is no change of the phase relations due to Si solution (Figure 4) and the D0_{22} -phase remains the ground state.

Interestingly, the formation energies for Si solution at the Al1 sites are lower than the corresponding one at the Al2 sites in $\text{D0}_{22}\text{-Al}_3\text{V}$. This is opposite to the cases in $\text{D0}_{22}\text{-Al}_3\text{Sc}$ and Al_3Ti .

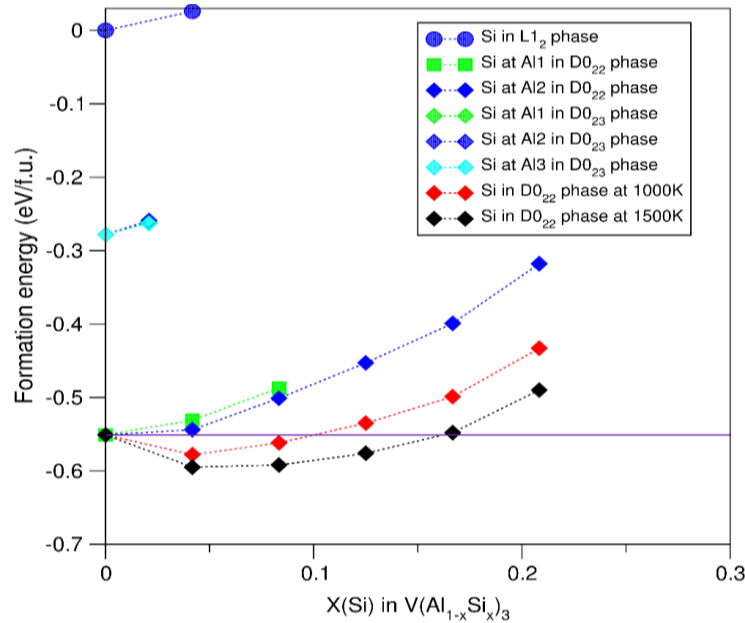


Figure 4. Relationships between the calculated formation energies and Si contents for the Al_3V phases. Clearly, Si solution in the phases is not favored with moderate costs for Si solution in $\text{D0}_{22}\text{-Al}_3\text{V}$. The Si solution occurs at elevated temperatures due to thermodynamic contribution.

Figure 4 shows that for $\text{D0}_{22}\text{-Al}_3\text{V}$ the costs for Si solution in this phase are moderate. It is reasonable to consider its stability at elevated temperatures. Configurational entropy contributions were estimated for Si solutions at the Al sites in $\text{D0}_{22}\text{-Al}_3\text{V}$ using the same approach in subsection 3.3.2. The obtained data for the Gibbs energies at 1000 K (about the casting temperature) and 1500 K (around the formation temperature of Al_3V phase [6]) were plotted into Figure 4.

The Si regions of negative Gibbs energy of the system are about 11 at.% at 1000K and 17 at.% at 1500 K, respectively. Therefore, $\text{D0}_{22}\text{-(Al,Si)}_3\text{V}$ may be formed and stable at elevated temperatures.

Overall, Si solution in Al_3V is not favored. Meanwhile, energy costs for Si solution in $\text{D0}_{22}\text{-(Al,Si)}_3\text{V}$ are moderate, indicating occurrence of Si solution at high temperatures. Naturally, the Si content in a prepared sample depends on the chemical composition and the experimental conditions.

3.4 Crystal chemistry of the $(\text{Al}_{1-x}\text{Si}_x)_3\text{T}$ phases

3.4.1 Structural properties of the highly stable (Si-doped) Al_3T phases

The present first-principles calculations showed a rich variety of Si stabilization effects in Al_3T phases. The binary cubic $\text{L1}_2\text{-Al}_3\text{Sc}$ is the ground state and Si solution in this phase is energetically costly. Thus, Si content in $\text{L1}_2\text{-Al}_3\text{Sc}$ is moderate even at elevated temperatures. Meanwhile, Si solution at the Al sites in $\text{D0}_{22}\text{-Al}_3\text{Ti}$ is favored. Si solution in $\text{D0}_{22}\text{-Al}_3\text{V}$ costs only moderate energies and thus, occurs at elevated temperatures. Therefore, it is likely to obtain $\text{D0}_{22}\text{-(Al}_{1-x}\text{Si}_x)_3\text{V}$ samples via e.g. quenching approaches. The influences of Si content in the $\text{D0}_{22}\text{-(Al}_{1-x}\text{Si}_x)_3\text{T}$ ($\text{T} = \text{Ti, V}$) on their crystal structures become important for characterizing the phase in Al alloys. The relationships between the lattice parameters and Si contents for the $\text{D0}_{22}\text{-Al}_3\text{T}$ ($\text{T} = \text{Ti}$ and V) are presented in Figure 5.

As shown in Figure 5, the lattice parameters and the corresponding volumes for both $\text{D0}_{22}\text{-Al}_3\text{T}$ ($\text{T} = \text{Ti}$ and V) systems decrease with increasing Si content in common. This general trend is in line with the smaller atomic radius for Si (1.15 Å) than that of Al (1.43 Å) [53] and with the calculations that the shorter Al-Si bonds for the dilute Si solute in Al (1.84 Å) than that of the Al-Al bonds (1.86 Å) (Table I).

Figure 5a shows that for $\text{D0}_{22}\text{-(Al}_{1-x}\text{Si}_x)_3\text{Ti}$, the length of the a -axis for the configurations with Si at Al2 decreases more rapidly than that for those with Si at the Al1 (2b) sites. Opposite behavior was uncovered for the c -axis which length decreases quicker for Si at the Al2 (4d) sites. The volume of the configurations with Si at Al1 decreases faster as well.

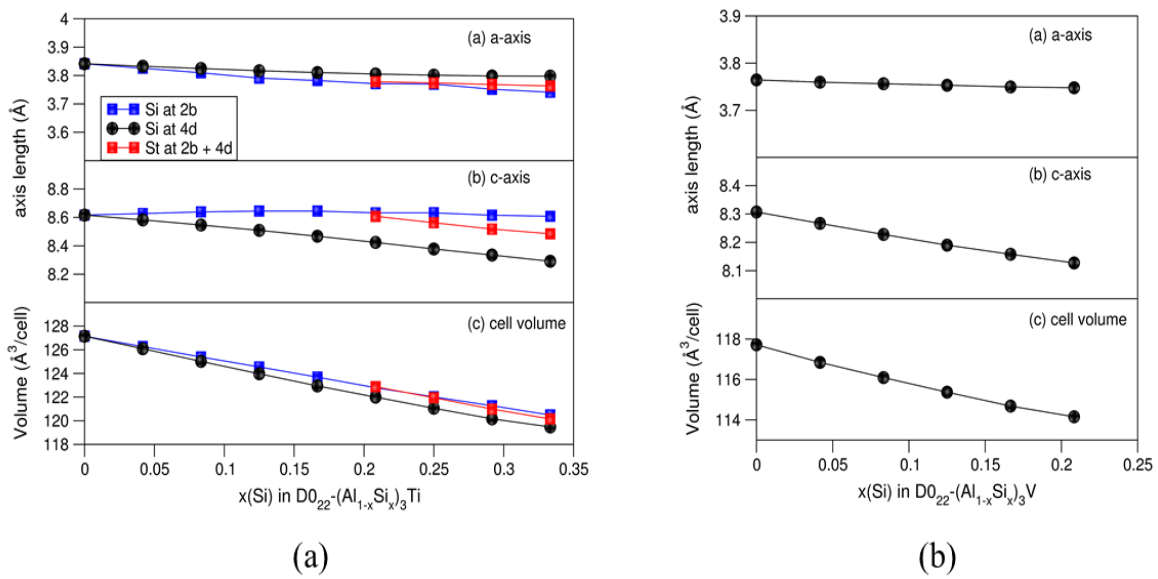


Figure 5. Dependences of lattice parameters and cell volumes on Si content at the Al1 and Al2 sites in $\text{D0}_{22}\text{-(Al}_{1-x}\text{Si}_x)_3\text{Ti}$ (a), and at the Al2 sites in $\text{D0}_{22}\text{-(Al}_{1-x}\text{Si}_x)_3\text{V}$ (b). Clearly lengths of the lattice parameters and the cell volumes decrease with increasing Si content.

The lattice parameters for the most stable configuration, $\text{D0}_{22}\text{-(Al}_{0.833}\text{Si}_{0.167})_3\text{Ti}$ with Si at the Al1 (Wyckoff 2b) sites are $a = 3.810$ Å and $c = 8.468$ Å, which are about 5.2 % and 3.8 %, respectively smaller than those of $\text{D0}_{22}\text{-Al}_3\text{Ti}$ (Table II). Figure 3 shows that at 1000 K the Gibbs energies are moderate in the range of Si contents (x) from 0.125 to 0.333, in which the a -/ c -axis have lengths between 3.79 Å/8.64 Å to 3.74 Å/8.61 Å for Si at the Al1 sites and 3.82 Å/8.52 Å to 3.80 Å/8.2 Å for Si at the Al2 sites (Figure 5), respectively. This helps understand the rich variation of the lattice parameters from the experiments [27,33-35].

Si solution in $\text{D0}_{22}\text{-Al}_3\text{V}$ is possible at elevated temperatures (Figure 4). The lattice parameters (a/c) decrease moderately from 3.764 Å/8.307 Å ($x(\text{Si}) = 0$) to 3.756 Å/8.227 Å ($x(\text{Si}) = 8.3$ %). The observation large range of the lattice parameters (Table II) in the experiments [36,51] may come from a different origin.

3.4.2 Electronic properties of and chemical bonding in the stable $(\text{Al}_{1-x}\text{Si}_x)_3\text{T}$ phases

Electronic band structure calculations were worked out for the highly stable $\text{L1}_2\text{-Al}_3\text{Sc}$, $\text{D0}_{22}\text{-(Al}_{0.833}\text{Si}_{0.167})_3\text{Ti}$ and $\text{D0}_{22}\text{-Al}_3\text{V}$ and meta stable $\text{D0}_{22}\text{-(Al}_{0.958}\text{Si}_{0.042})_3\text{V}$. The obtained local coordination of Sc by Al atoms in the $\text{L1}_2\text{-Al}_3\text{Sc}$ is shown in Figure 6a, while the electron density distributions in the rest of the above-mentioned phases are shown in Figures 6b to 6d. The curves of the related densities of states for $\text{D0}_{22}\text{-(Al}_{0.833}\text{Si}_{0.167})_3\text{Ti}$ and $\text{D0}_{22}\text{-Al}_3\text{V}$ and $\text{D0}_{22}\text{-(Al}_{0.958}\text{Si}_{0.042})_3\text{V}$ are shown in Figure 7, whereas the DOS curves for $\text{L1}_2\text{-Al}_3\text{Sc}$ and novel $\text{D0}_{22}\text{-Al}_3\text{Ti}$ are shown in Figure 8a and 8b respectively, with the latter for comparison.

The cuboctahedral coordination of Sc by Al in $\text{L1}_2\text{-Al}_3\text{Sc}$ is shown clearly in Figure 6a. Symmetries and the overlapping between the electron densities in the Al-V-Al chains in $\text{D0}_{22}\text{-Al}_3\text{V}$ in the a - b plane are presented in

Figure 6b. Figure 6c also shows the overlapping of electron clouds of Si with those of V, indicating local strong Si-V bonding. For $D0_{22}-(Al_{0.833}Ti_{0.167})_3Ti$, there are electron overlapping in the Ti-Si-Ti chains parallel to the b -axis, indicating chemical bonding between Ti and Si (Figure 6d).

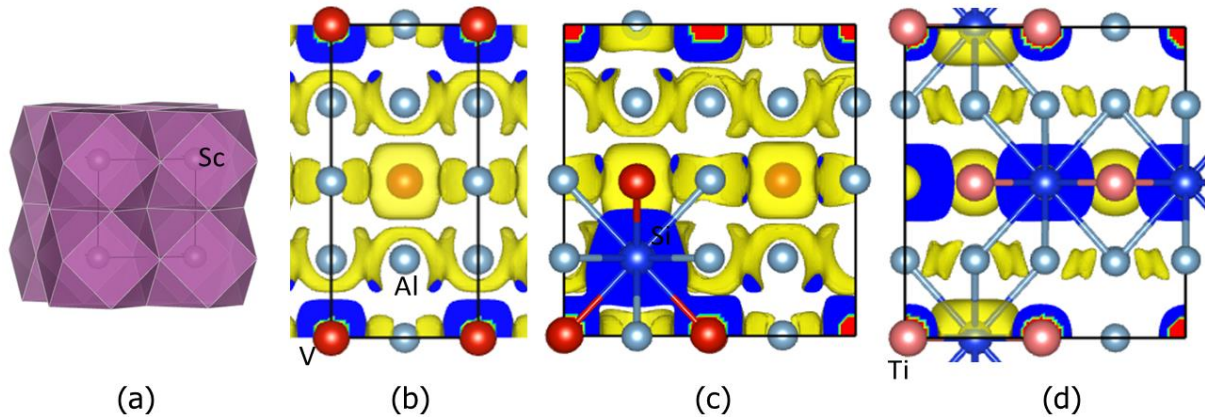


Figure 6. Schematic coordination and electron density distributions in $L1_2-Al_3Sc$ (a), $D0_{22}-Al_3V$ (b), $D0_{22}-(Al_{0.958}Si_{0.042})_3V$ (c) and $D0_{22}-(Al_{0.833}Si_{0.167})_3Ti$ (d) along (approximately for a) the $[100]$ orientation. The black lines represent the b -axis (horizontal) and c -axis (vertical). The bonds between Si and T/Al are shown for the Si doped systems (c) and (d).

The curves of the calculated partial density of states for the Al and Sc atoms in and the total density of states of $L1_2-Al_3Sc$ are shown in Figure 8a. The present calculated results agree with the previous calculations by Duan et al. who employed the first-principles density functional theory within the local-density approximation [54]. The Al 3s states dominate the lower part of the valence band (-10.0 eV to -3.0 eV) (Figure 8a) while the DOS curve around the Fermi level is dominated by Sc 3d states mixed with Al 3p states (from -3.0 eV to the Fermi level, zero eV). There is a broad valley ranging from -0.9 eV to +0.5 eV in which the Fermi level falls. Such low DOS at the Fermi level indicates electronic stability of this crystal according to Stoner's theory [55]. This agrees with the energy cost for Si solution.

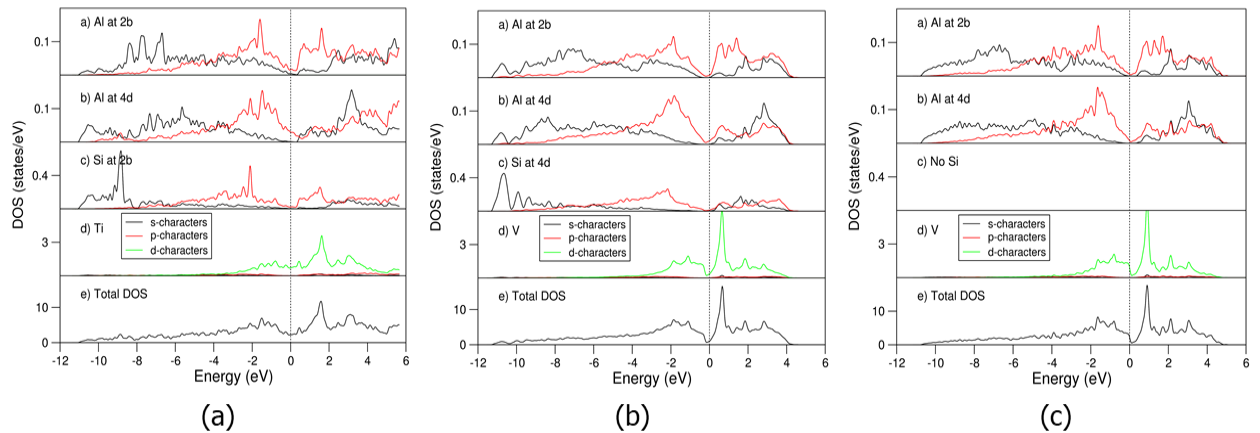


Figure 7. Partial density of states of selected atoms (pDOS) in and total density of states (tDOS) of the highly stable $D0_{22}-(Al_{0.833}Si_{0.167})_3Ti$ (a), $D0_{22}-Al_3V$ (c) and $D0_{22}-(Al_{0.958}Si_{0.042})_3V$ (b). The unit is states/eV per atom for the pDOS curves and states/eV per primitive unit cell for the tDOS curves. The vertical dotted lines at zero eV represent the Fermi level.

Figure 7c shown the DOS curves for $D0_{22}-Al_3V$. The DOS curves can be divided into a valence band (from -10.7 eV to 0.0 eV) and the conduction band above the Fermi level above with a pseudo-gap in-between. The lower part of the valence band (from the bottom to -3.0 eV) is dominated by Al 3s states while the upper part (-3.0 eV to 0.0 eV) is dominated by V 3d and Al 3p states. The Fermi level is just at the starting of the valley which is determined by the V 3d states.

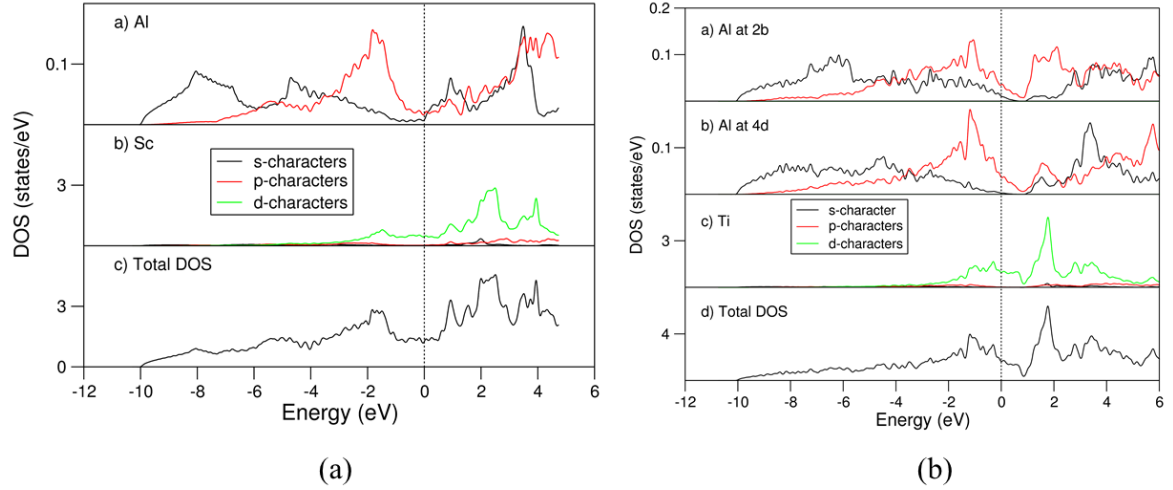


Figure 8. pDOS in and tDOS of $L1_2$ - Al_3Sc (a) and novel $D0_{22}$ - Al_3Ti (b). The unit is states/eV per atom for the pDOS curves and states/eV per primitive unit cell for the tDOS curves. The vertical dotted lines at zero eV represent the Fermi level.

The overall shapes of the DOS curves for the Si doped, $D0_{22}$ - $(Al_{0.958}Si_{0.042})_3V$ (Figure 7b) are similar to the corresponding binary Al_3V (Figure 7c). A close look reveals differences. First addition of Si causes lowering of the valence band to -11.3 eV. This is due to mixing of the Si 3s states which dominated the lower part of the valence band from -11.3 eV to -8.0 eV with the Al 3s states. Secondly, the Fermi level shifts from the start of the DOS valley to its middle (Figure 7b) from the beginning of the DOS curve in the parent binary (Figure 7c). The higher DOS at the parent $D0_{22}$ - Al_3V (Figure 7c) might be the cause of moderate Si solution at the Al sites, which may shift the Fermi level to the middle of the DOS valley dominated by V 3d states to enhance the stability of the compound.

The overall shapes of the DOS curves of $D0_{22}$ - $(Al_{0.833}Si_{0.167})_3Ti$ (Figure 7a) are also similar to the corresponding ones of $D0_{22}$ - $(Al_{0.958}Si_{0.042})_3V$ (Figure 7b). Meanwhile some subtle differences can be recognized: a) the Si 3s states show more localized between the bottom to -8.0 eV in the valence band in the former as compared to those in the latter; b) The sum of the occupied Ti 3d states in Figure 7a is notably smaller than that in Figure 7b, indicating more 3d electron in V and in Ti. The tDOS curve around the Fermi level in $D0_{22}$ - $(Al_{0.833}Si_{0.167})_3Ti$ is dominated by Ti 3d state and form a plateau with electron density of states at Fermi level being 0.71 states/eV for Ti 3d states. In comparison the total DOS curve of the binary $D0_{22}$ - Al_3Ti has a deep valley at 0.86 eV (See Figure 8b). Using rigid band filling model, we may conclude that replacement of Al by Si adds electrons into the system, shifts the Fermi level at a high density of the binary compound (Figure 8b) to the DOS valley at a higher energy (Figure 7a), which enhances the stability of the system according to the criteria [55]. This is the physics behind the stability effect of Si solution in $D0_{22}$ - Al_3Ti .

3.5 Electron count and the $(Al_{1-x}Si_x)_3T$ phases

The early 3d transition metals belong to the s-d elements with electronic configurations: Sc [Ar] $3d^1 4s^2$, Ti [Ar] $3d^2 4s^2$, and V [Ar] $3d^3 4s^2$, here [Ar] represents the close-shell core electrons. Our calculations showed a trend between the electron number and the energetic hierarchy of the phases: by increasing electron number, the preferred structure is $L1_2$ for $ScAl_3$ to $D0_{23}$ for $TiAl_3$, and to $D0_{22}$ for VAl_3 . Analogous behavior is expected for the related TAl_3 compounds with T = the early 4d/5d transition metals (Y/Lu; Zr/Hf and Nb/Ta) [39, 43, 52, 56]. Such an energetic hierarchy and phase relations have been confirmed by our systematic first-principles calculations for the TAl_3 family (Table III) with the same code and settings described in Section 2.

Table III Calculated formation energies (ΔE_f) for the TAl_3 (T = Sc/Y/La, Ti/Zr/Hf, V/Nb/Ta) phases and related electronic configurations of the early nd ($n = 3, 4, 5$) transition metals according to Equation 1. The most stable phases are marked in **bold**.

Phase	Formation energy ΔE_f (eV/f.u.) and related electronic configurations of T								
	Al_3Sc ($3d^1 4s^2$)	Al_3Ti ($3d^2 4s^2$)	Al_3V ($3d^3 4s^2$)	Al_3Y ($4d^1 5s^2$)	Al_3Zr ($4d^2 5s^2$)	Al_3Nb ($4d^3 5s^2$)	Al_3La ($5d^1 6s^2$)	Al_3Hf ($5d^2 6s^2$)	Al_3Ta ($5d^3 6s^2$)
$L1_2$	0.00	0.00	0.00	0.00	0.00	0.00	0.00	0.00	0.00
$D0_{22}$	0.36	-0.11	-0.54	0.51	0.00	-0.66	0.59	-0.08	-0.67
$D0_{23}$	0.18	-0.13	-0.27	0.26	-0.10	-0.33	0.28	-0.11	-0.34

1 Table III shows clearly the relation between the preferred structure and electron count in the TAl_3 family.
2 With increasing number of electrons, the preferred structure transits from $L1_2$ - for $T = Sc/Y/La$ (d^1 elements) to
3 $D0_{23}$ for $T = Ti/Zr/Hf$ (d^2) and further to $D0_{22}$ for $T = V/Nb/Ta$ (d^3).

4 Si replacing Al in TAl_3 indicates increasing number of electrons in the system and corresponding, it may
5 cause phase changes. This is exemplified by Si dissolving at the Al1 sites in $D0_{22}$ - $ScAl_3$ (Figure 2). The
6 remarkable stabilization effect is Si dissolving in $D0_{22}$ - $TiAl_3$. As shown in Figure 3, a moderate content of
7 dissolving Si causes transition from the $D0_{23}$ - $TiAl_3$ to $D0_{22}$ - $Ti(Al_{1-x}Si_x)_3$ ($x > 0.02$). For $D0_{22}$ - VAl_3 , Si dissolving
8 has little stabilization effect, since it contains already the highest number of electrons for this family. Naturally
9 such stabilization effect due to increasing number of electrons holds for the related TAl_3 with $T = Y/La, Zr/Hf$
10 and Nb/Ta .

11 Table III shows also notable energetic differences for the TAl_3 phases with different transition metals. For
12 example, the energy difference between $D0_{22}$ - and $D0_{23}$ - $TiAl_3$ is about 0.02 eV/f.u. which is notably smaller
13 than that for $ZrAl_3$ (0.10 eV/f.u.). Correspondingly, the minimal Si content for the stabilized $D0_{22}$ - $Ti(Al_{1-x}Si_x)_3$ is
14 small ($x \sim 0.02$), whereas it will be larger for stabilizing the $D0_{22}$ - $Zr(Al_{1-x}Si_x)_3$ over the $D0_{23}$ - $ZrAl_3$. Moreover,
15 replacing Al by an element with less valence electrons, such as alkaline earth or noble metal elements reduces
16 the electrons in the system, which may change the energetic hierarchy and the phase relation in the TAl_3
17 compounds in a reverse way. Effects of impurity solution in the TAl_3 compounds listed in Table III and for $T =$
18 e.g. $Cr/Mo/W$ (d^4) elements, deserve further investigation.

21 4. Conclusions

22 First-principles density-function theory calculations for Si solution on the $L1_2$ -, $D0_{22}$ - and $D0_{23}$ - Al_3T ($T =$
23 Sc, Ti and V) phases showed that Si prefer uniformly distribution in the same type of Al site. Si solution has a
24 rich variety of effects on the stability of the Al_3T phases.

25 There is a link between the number of electrons in TAl_3 and the preferred structures: $L1_2$ - $ScAl_3$, $D0_{23}$ - $TiAl_3$
26 and $D0_{22}$ - VAl_3 . Si replacing Al increases the number of electrons in the systems, which may cause change of the
27 corresponding preferred structures. This link also holds for the corresponding early 4d and 5d transition metal
28 tri-aluminides.

29 Si solution stabilizes $D0_{22}$ - Al_3Ti phase so that the Si partially dissolved phase it goes by the binary $D0_{23}$ -
30 Al_3Ti . The partial substitution also induces extra freedom for the Si content at high temperatures. This explains
31 the widely observed $D0_{22}$ -type particles in the commercial Al-based alloys which contains variable degrees of
32 Si. The most stable configuration has chemical formula, $D0_{22}$ - $(Al_{0.833}Si_{0.167})_3Ti$.

33 Si can be dissolved at the Al1 and Al2 sites in and stabilize both $D0_{22}$ - and $D0_{23}$ - Al_3Sc phases. However, the
34 Si stabilization is not enough to change their phase relations that the binary $L1_2$ - Al_3Sc structure keeps the
35 ground state phase. The high energy cost indicates low Si doping in the cubic $L1_2$ - Al_3Sc crystals even at
36 elevated temperatures.

37 Si solution is not favored in the Al_3V phases. Meanwhile, the energy cost for Si solution in the $D0_{22}$ -phase is
38 moderate. Therefore, configurational entropy contribution enables moderate Si solution in $D0_{22}$ - Al_3V at elevated
39 temperatures.

40 Crystallographically, Si solution reduces the lattice parameters in an almost linear way. This agrees with the
41 rich variation of the lattice parameters for the $D0_{22}$ - $(Al,Si)_3Ti$ phase observed in the manufactured Al alloys.

42 The electronic structure calculations showed that strong bonding between Si and the transition metals. The
43 Fermi level falls in the DOS valleys for the highly stable $L1_2$ - Al_3Sc , $D0_{22}$ - $(Al_{0.833}Si_{0.167})_3Ti$ and Si moderately
44 doped $D0_{22}$ - $(Al_{1-x}Si_x)_3V$ (e. g. $x \sim 0.04$) phases.

49 Acknowledgements

50 The authors thank Dr. Yun Wang (BCAST) for beneficent discussions. Financial support from EPSRC (UK)
51 under grant number EP/V011804/1 and EP/S005102/1 is gratefully acknowledged.

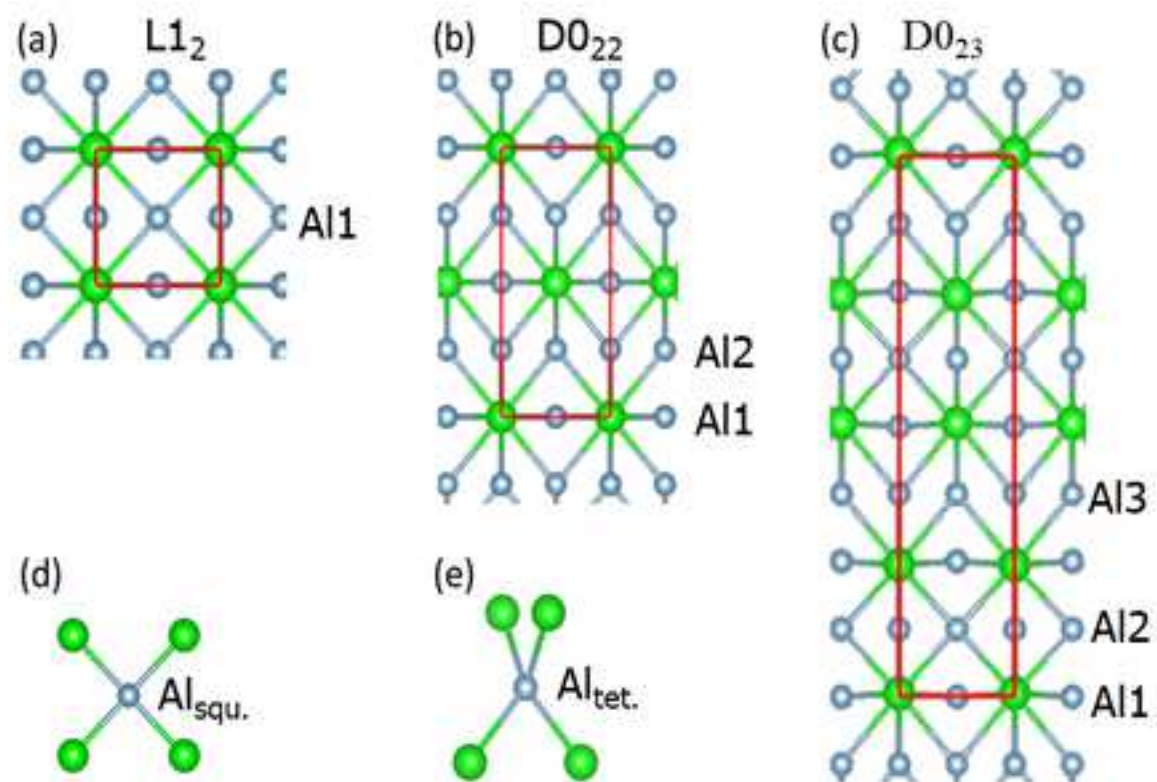
55 Conflict of Interest

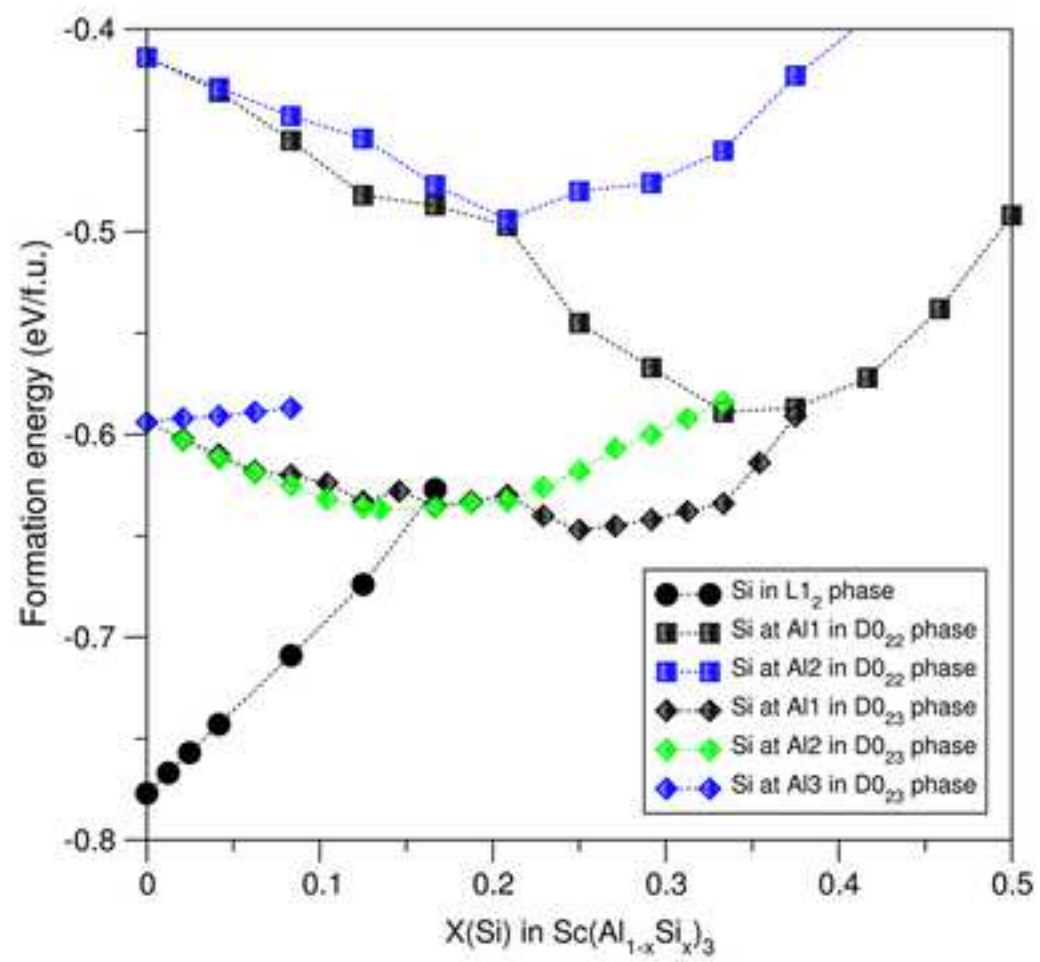
56 The authors declare that they have no conflict of interest.

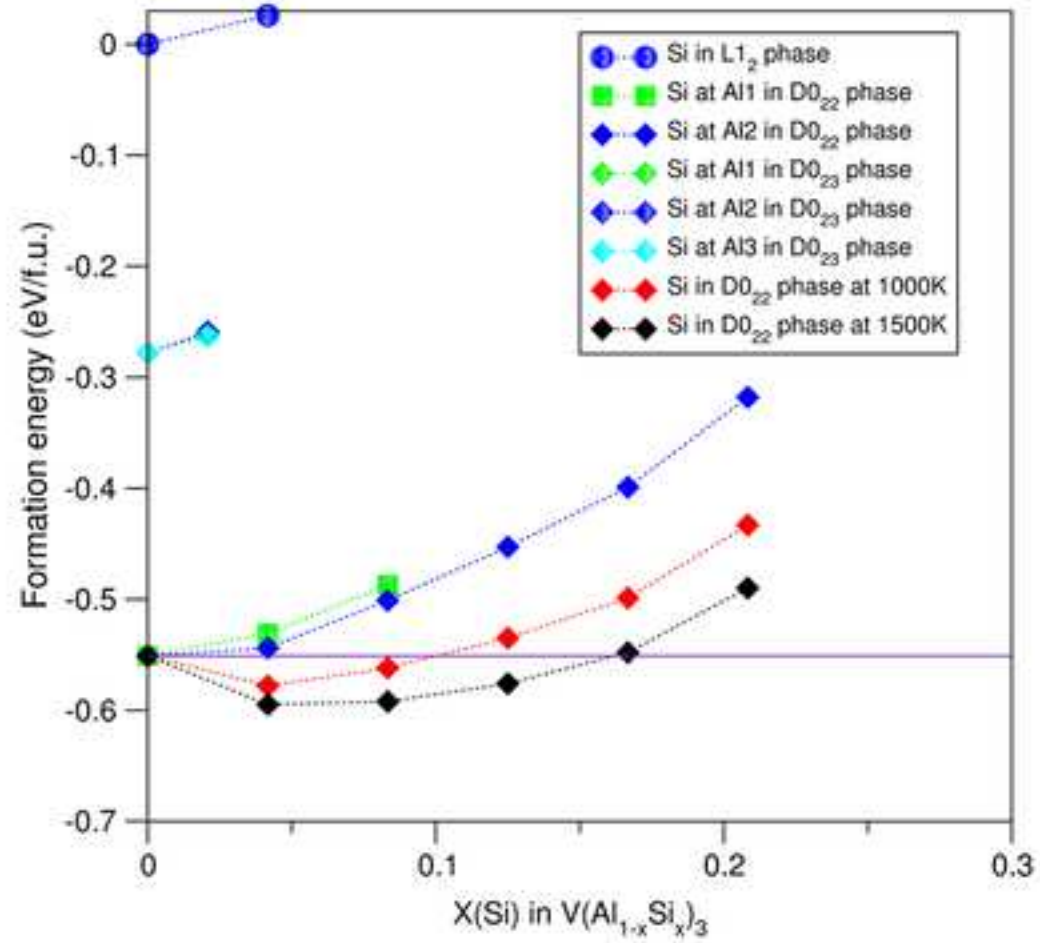
References

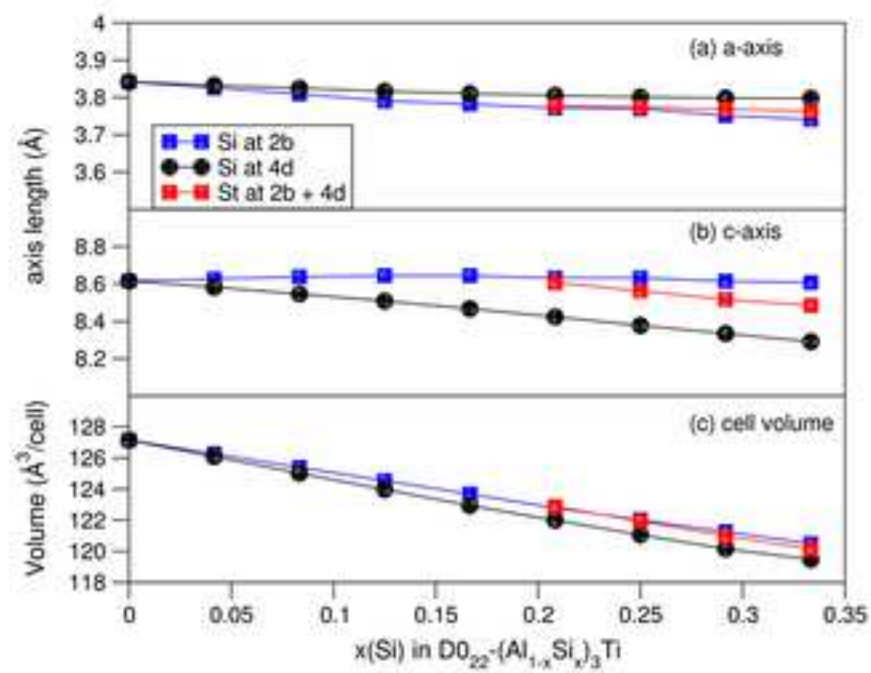
- 1) J.-F. Nie, *Physical metallurgy of light alloys*, in: D.E. Laughlin, K. Hono (Eds.), *Physical Metallurgy*, fifth ed., Elsevier, Oxford (UK), 2014.
- 2) M. V. Glazoff, A. V. Khvan, V. S. Zolotarevsky, N. A. Belov and A. T. Dinsdale, *Casting aluminum alloys*, Butterworth-Heinemann (Elsevier), Kidlington (UK)/Cambridge (USA) 2019.
- 3) J. W. Arblaster, *Selected values of the crystallographic properties of elements*, ASM International, Materials Park, Ohio (USA), 2018.
- 4) J. L. Murray, *J. Phys. Equilib.* II 19, 380 (1998).
- 5) V. Raghavan, *J. Phys. Equilib. Diffus.* 26, 171 (2005).
- 6) H. Okamoto, *J. Phys. Equilib. Diffus.* 33, 491 (2012).
- 7) S. K. Shaha, F. Czerwinski, W. Kasprzak, J. Friedman and D. K. Chen, *Metal. Mater. Trans. A* 47A, 2396 (2016).
- 8) M. Ožko, E. Babić, R. Krsnik, E. Girt and B. Leontić, *J. Phys. F: Metal Phys.* 6, 703 (1976).
- 9) J. Røyset and N. Ryum, *Intern. Mater. Rev.* 50, 19 (2015).
- 10) D. N. Seidman, E. A. Marquis and D. C. Dunand, *Acta Mater.* 50, 4021 (2002).
- 11) S. Z. Anvari, F. Karimzadeh and M. H. Enayati, *Mater. Sci. Technol.* 34, 179 (2018).
- 12) Y. B. Wang, Z. Y. Huang, W. Q. Hu, L. P. Cai, C. Lei, Q. Yu and Y. D. Jiao, *Mater. Charac.* 178, 111298 (2021).
- 13) C. Booth-Morrison, D. C. Dunand and D. N. Seidman, *Acta Mater.* 59, 7029 (2011).
- 14) K. Yan, Z. W. Chen, Y. N. Zhao, C. C. Ren, W. J. Lu and A. W. Aldeen, *J. Alloys Compd.* 861, 158491 (2021).
- 15) M. F. Liu, C. S. Zhang, Z. J. Meng, G. Q. Zhao and L. Chen, *Composites Part B* 226B, 109331 (2021).
- 16) Y. Meng, Y. Yang, C. Li, L.-G. Cao, Z.-H. Zhao, Q.-F. Zhu and J.-Z. Cui, *Trans. Nonferrous Met. Soc. China* 32, 2110 (2022).
- 17) G. M. A. Mahran and A.-N. M. Omran, *Mater. Sci. (Medžiagotyra)* 28, 41 (2022).
- 18) M. Easton and D. StJohn, *Metall. Mater. Trans. A* 30A, 1613 (1999).
- 19) G. S. Vinod Kumar, B. S. Murty and M. Chakraborty, *J. Mater. Sci.* 45, 2921 (2010).
- 20) P. Schumacher, A. L. Greer, J. Worth, P. V. Evans, M. A. Kearns, P. Fisher and A. H. Green, *Mater. Sci. Technol.* 14, 394 (1998).
- 21) Z. Fan, Y. Wang, Y. Zhang, T. Qin, X. R. Zhou, G. E. Thompson, T. Pennycook and T. Hashimoto, *Acta Mater.* 84, 292 (2015).
- 22) J. H. Li, F. S. Hage, Q. M. Ramasse and P. Schumacher, *Acta Mater.* 206, 116652 (2021).
- 23) F. Foadian, M. Soltanieh, M. Adeli and M. Etmianbakhsh, *Metall. Mat. Trans. B* 47B, 2931 (2016).
- 24) J. Atherton, *Int. J. Life Cycle Assess.* 12, 59 (2007).
- 25) D. Raabe, D. Ponge, P. J. Uggowitzer, M. Roscher, M. Paolantonio, C. L. Liu, H. Antrekowitsch, E. Kozenschnik, D. Seidmann, B. Gault, F. De Geuser, A. Deschamps, C. Hutchinson, C. H. Liu, Z. M. Li, P. Prangnell, J. Robson, P. Shanthraj, S. Cakili, C. Sinclair and S. Pogatscher, *Prog. Mater. Sci.* 128, 100947 (2022).
- 26) R. W. G. Wyckoff, *Crystal Structures*, John Wiley, New York (USA), 1963.
- 27) C. M. Fang and Z. Fan, *Comp. Mater. Sci.* 153, 309 (2018).
- 28) X. Y. Zhang, Y. C. Huang, Y. Liu, and X. W. Ren, *Results in Physics* 19, 103378 (2020).
- 29) Z. Chen, P. Zhang, D. Chen, Y. Wu, M. L. Wang, N. H. Ma and H. W. Wang, *J. Appl. Phys.* 117, 085904 (2015).
- 30) C. Amador, J. J. Hoyt, B. C. Chakoumakos and D. de Fontaine, *Phys. Rev. Lett.* 74, 4955 (1995).
- 31) J. C. Schuster and M. Palm, *J. Phase Equilib. Diffus.* 27, 255 (2006).
- 32) J. L. Murray, *Binary Alloys Phase Diagrams*, in: T. G. Massalski (Ed.), ASM, Metals Park, Ohio (USA), 1986.
- 33) F. J. J. van Loo and G. D. Rieck, *Acta Metallurgica* 56, 61 (1965).
- 34) S. Srinivasan, P. B. Desch and R. B. Schwarz, *Scripta Metall. Mater.* 125, 2513 (1991).
- 35) M. H. Lee, J. Lee and Z.-H. Lee, *Scripta Metal.* 25, 517 (1991).

- 1
2
3
4
5
6
7
8
9
10
11
12
13
14
15
16
17
18
19
20
21
22
23
24
25
26
27
28
29
30
31
32
33
34
35
36
37
38
39
40
41
42
43
44
45
46
47
48
49
50
51
52
53
54
55
56
57
58
59
60
61
62
63
64
65
- 36). R.B. Schwartz, P.B. Desch, S. Srinivasan, *Static and Dynamics of Alloys Phase Transformation*, Plenum Press, New York (USA), 1994.
 - 37). C. M. Fang, Z. P. Que and Z. Fan, *J. Solid State Chem.* 299, 122199 (2021).
 - 38). Z. Li, C. L. Liao, X. M. Wang, Y. Wu, M. X. Zhao, Z. H. Long and F. C. Yin, *J. Phase Equilib. Diffus.* 35, 564 (2014).
 - 39). J.-R. Castillo-Sánchez, G. Salloum-Abou-Jaoude, A. E. Gheribi, P. Lafaye, K. Oishi, J.-P. Masse, E. Bousser, G. L'Espérance and J.-P. Harvey, *Acta Mater.* 262, 119455 (2023).
 - 40). R. Boulechfar, D. Sayad, Y. Khenioui, H. Meradji, S. Ghemid, R. Kenata, S. Bin-Omran, A. Bouhemadou and S. Goumri-Said, *Eur. Phys. J. B* 97B, 1(2024).
 - 41). Z. Ahmad, *J. Metals* 55, 35 (2003).
 - 42). Y. Harada and D. C. Dunand, *Mater. Sci. Engin. A* 329-331A, 686 (2002).
 - 43). J. Dumre, S. K. Kairy, E. Anber, T. Langan, M. L. Taheri, T. Dorin and N. Birbilis, *J. Alloys Compd.* 861, 158511 (2021).
 - 44). Q. Yao, *Adv. Mater. Res.* 284-286, 1987(2011).
 - 45). G. Kresse and J. Furthmüller, *Comp. Mater. Sci.* 6, 15 (1996).
 - 46). J. P. Perdew, K. Burke, and M. Ernzerhof, *Phys. Rev. Lett.* 77, 3865 (1996).
 - 47). P. E. Blöchl, *Projector augmented-wave method*, *Phys. Rev. B.* 50B, 17953 (1994).
 - 48). C. M. Fang, Z. P. Que, A. Dinsdale and Z. Fan, *Intermetallics* 126, 106939 (2020).
 - 49). C. M. Fang, M. A. van Huis, M. H. F. Sluiter, and H. W. Zandbergen, *Acta Mater.* 58, 2968 (2010).
 - 50). H. J. Monkhorst and J. D. Pack, *Phys. Rev. B.* 13B, 5188 (1976).
 - 51). N. Blake and M. A. Hopkins, *J. Mater. Sci.* 20, 2861 (1985).
 - 52). M. Zedalis and M. E. Fine, *Script Metall.* 17, 1247 (1983).
 - 53). S. Guo and C. T. Liu, *Prog. Nat. Sci: Mater. Intern.* 21, 433 (2011).
 - 54). Y.-H. Duan, B. Huang, Y. Sun, M.-J. Peng and S.-G. Zhou, *Chin. Phys. Lett.* 31, 088101 (2014).
 - 55). E. C. Stoner, *Proc. Royal soc. A* 165A, 372 (1938).
 - 56). W.-S. Chang and B. C. Muddle, *Metals and Mater.* 3, 1 (1997).

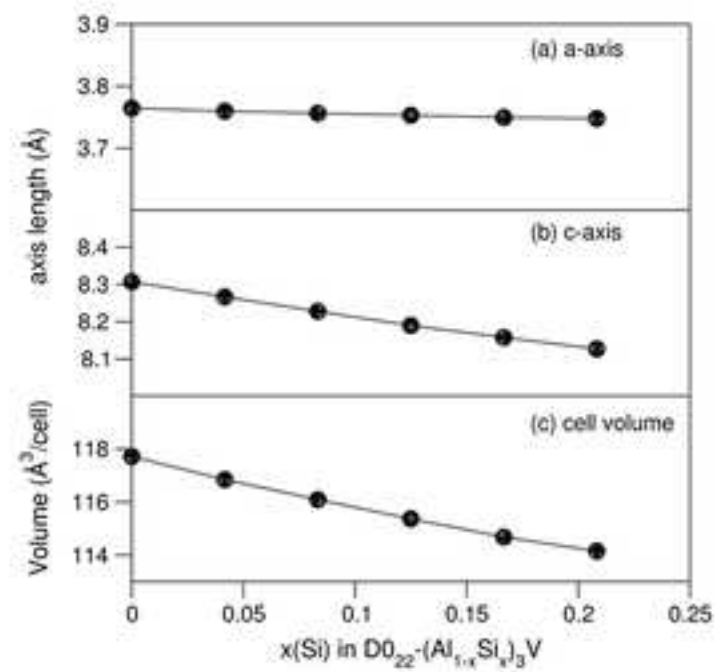




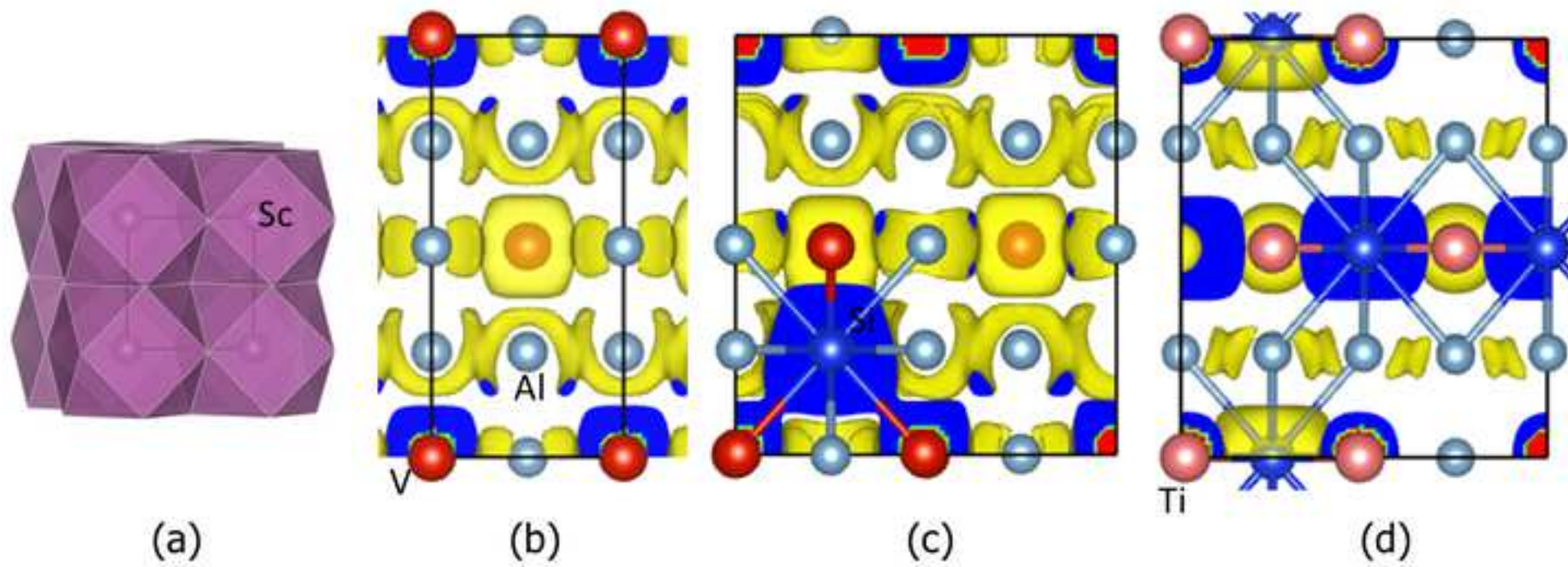


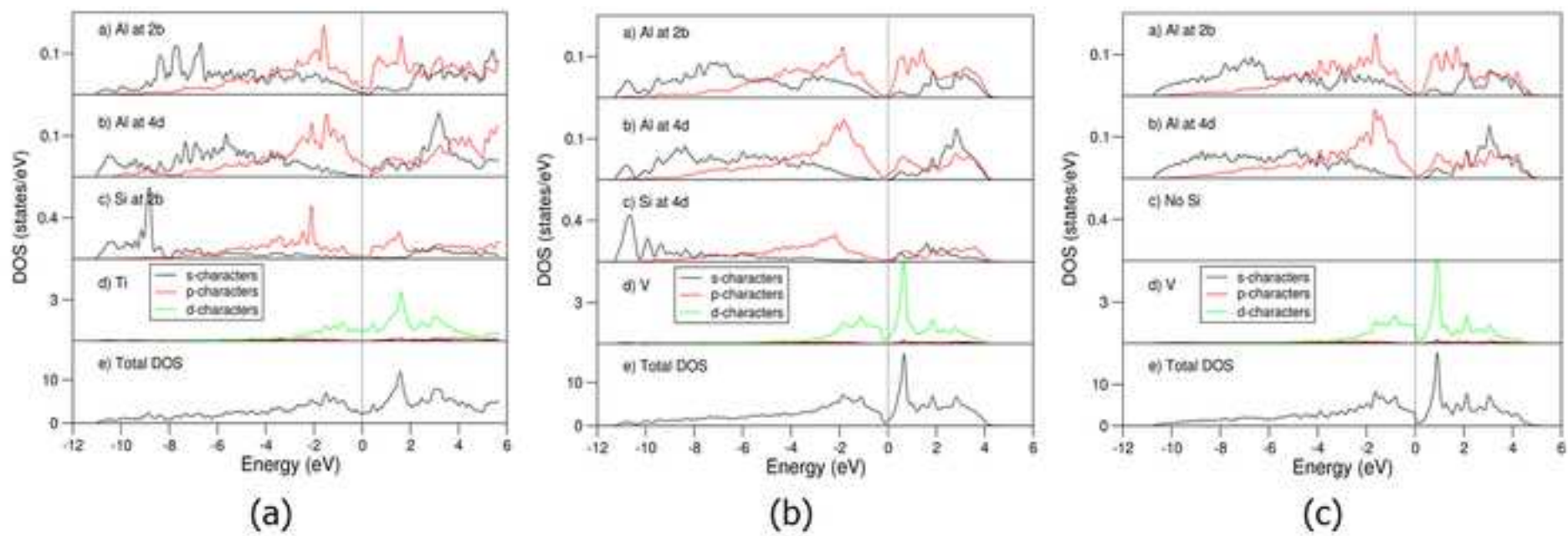


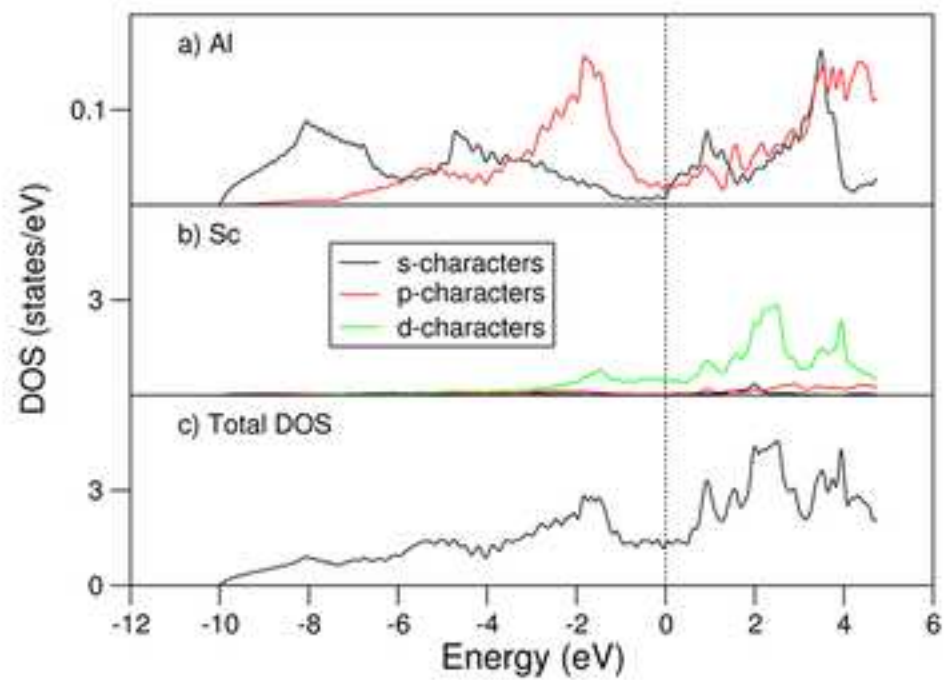
(a)



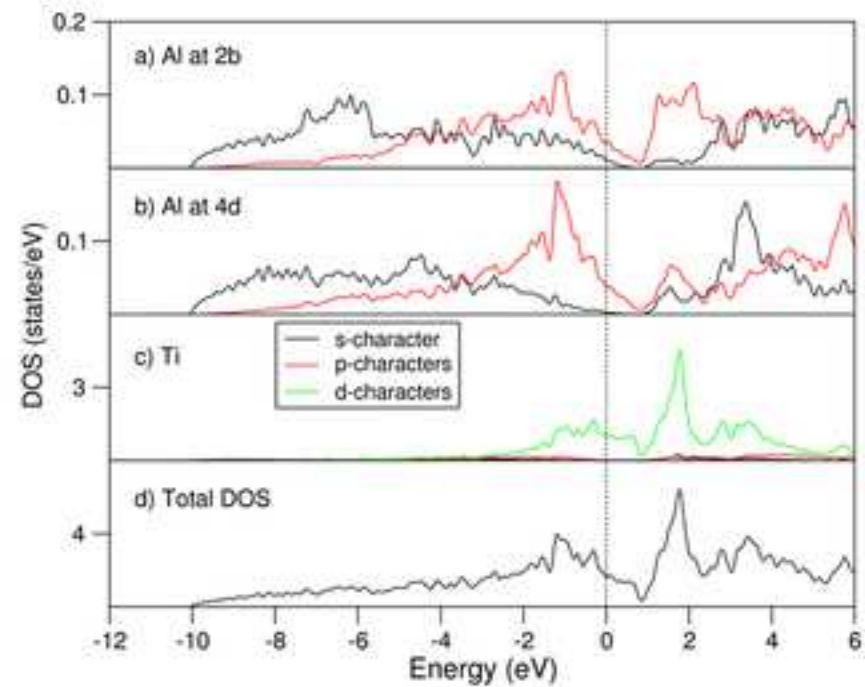
(b)







(a)



(b)

Effects of Si Solution on Stability of Early 3d Transition-Metal Tri-Aluminides, Al₃T (T = Sc, Ti and V)

C. M. Fang*, Z. P. Que and Z. Fan

Brunel Centre for Advanced Solidification Technology (BCAST), Brunel University London, Uxbridge, Middlesex UB8 3Ph, UK

* Corresponding author, e-mail: changming.fang@brunel.ac.uk

Abstract

Addition of the early 3d transition-metals results in formation of primary Al_3T (T = Sc, Ti and V) phases in Al alloys during casting. The newly formed Al_3T particles not only improve the mechanical performance of the products, but also act as grain-refiners in the solidification processes. Meanwhile, experiments found impacts of impurities, such as Si on the formation of the Al_3T phases, which mechanism is not fully understood. We here investigate effects of Si solution on the stability and crystal chemistry of the Al_3T phases using first-principles density-functional theory. The study has revealed a rich variety of effects of Si solution on the Al_3T phases. Si solution stabilizes the D0_{22} - Al_3Ti structure so that it becomes the ground-state, taking over the binary D0_{23} -phase. Si solution in D0_{22} -V occurs only at elevated temperature. Si solution has little impact on the Al_3Sc phase relationship. The obtained information helps characterize the $(\text{Al},\text{Si})_3\text{T}$ particles in Al products, understand their role in solidification and further design new Al alloys of desirable properties.

Key words: Aluminium; Si solution; transition metal tri-aluminites; phase relations; density functional theory.

1. Introduction

Addition of transition metals can improve the mechanical performance and corrosion resistance of Al alloys [1,2]. The early 3d transition metals have relatively low mass densities (3.0 g/cm^3 for Sc, 4.5 g/cm^3 for Ti and 6.1 g/cm^3 for V) which are comparable to that of Al (2.7 g/cm^3) [1,3]. This unusual character benefits manufacturing light-metal alloys of relatively small weight/volume ratios. The added early 3d transition metals during casting react with Al, forming Al_3T particles [4-7]. The newly formed micro-/nano-scaled Al_3T particles cause the enhanceimprovement of the mechanic performance and chemical properties of the products for aerospace and automotive transport applications [7-12].

Those native Al_3T particles may act as potential grain-refiners during solidification of the Al alloys, as well [13-17]. The small lattice mismatch between the cubic $\text{L}_{12}\text{-Al}_3\text{Sc}$ [8] and $\alpha\text{-Al}$ [3] means high nucleation potency of $\text{L}_{12}\text{-Al}_3\text{Sc}$ as nucleation sites substrates. Al_3Ti particles have been considered to act as a grain-refiner separately [18,19] or to work together with TiB_2 particles in the widely used Al-nTi-B ($n = 3, 5$) master alloys [20-22]. Native Al_3V particles perform grain-refinements in the Al(V) alloy [16,17]. Moreover, the early 3d transition metals tri-aluminides may also be formed at the joints during welding, e.g. Al_3Ti at Ti-containing metals/Al joints [23]. Thus, it is vital to have a comprehensive understanding about the phase relations, crystal structure and physical properties for furthering development of Al alloys of desirable properties, particularly for the recycling Al scrap/waste parts which may contain various impurities [24,25].

There are three most-likely phases for the tri-aluminides, the cubic L_{12} - and the tetragonal D_{022} - and D_{023} - Al_3T for $\text{T} = \text{Sc}, \text{Ti}$ and V [26,27]. The terms ' Al_3T ' and ' TAl_3 ' are exchangeable in rest of the paper. Their structures are schematically drawn in Figure 1.

In the cubic $\text{L}_{12}\text{-Al}_3\text{T}$ structure (Figure 1a), each T atom has 12 Al nearest neighbors in cuboctahedral coordination. Each Al atom has also 12 neighbors (four T and eight Al) and is in square-planar coordination of T (Figure 1d).

In the tetragonal D_{022} -phase, all atoms are still in the ideal positions, but the symmetry is broken (Figure 1b). The T atoms are in distorted cuboctahedral coordination of Al. There are two types of Al coordination by T. One third of the Al atoms positioned in the same planes with T (with the coordinate component, $z = 0.0$ and 0.5 in Figure 1b) are in square-planar coordination by T (Figure 1d). The rest two-thirds (with $z = 0.25$ and 0.75) are tetrahedrally coordinated by T (Figure 1e).

In the D_{023} -phase, not only the symmetry is broken but also the atomic positions deviate from the ideal sites. The local coordination thus, becomes distorted. All the T are still in distorted cuboctahedral coordination by Al. One third of the Al atoms ($z = 0.375$ and 0.875 in Figure 1c) are in the distorted tetrahedral coordination by T and the other two thirds are in distorted square-planar coordination with the Al being out of the T planes.

Overall, the L_{12} , D_{022} and D_{023} structures (Figure 1) can be regarded as face-centred cubic (FCC) superstructures. The different coordination, broken symmetry and local structural distortion in the D_{022} - and D_{023} -phases would have impact on their stability and content of Si solution at the Al sites.

The phase relationships of the early 3d transition metal tri-aluminides have been a topic of intensive study both experimentally [4-7,26] and theoretically [27-29]. It is generally concurred that the ground state Al_3Sc has the cubic L_{12} -type structure (Figure 1a) [4,8,10,28], and Al_3V the tetragonal D_{022} -type structure [7,11,16,29].

There have been intensive discussions about the phase relations for Al_3Ti as summarized in [27]. The advanced first-principles calculations-investigations established that the D_{023} -phase is the ground state for Al_3Ti [27,30]. Meanwhile, the experiments produced a scattering of results. The thermodynamics study for the binary Al-Ti phase diagrams suggested phase transition between a high-temperature phase to a low-temperature one with variable transition temperatures [5, 27,31,32]. Structural characterization revealed formation of $\text{D}_{022}\text{-Al}_3\text{Ti}$ particles in manufactured Al products [33-35]. Furthermore, the lattice parameters for the Al_3Ti phases in different samples vary notably [27,33-35]. The latter is also true for the observed $\text{D}_{022}\text{-Al}_3\text{V}$ samples [35,36].

Impurities including Si exist inevitably in commercial Al metals [37]. Si is often added into Al to obtain products of desirable properties for applications at extreme conditions, e.g. high temperatures [1,2]. Hence it is necessary to have a good understanding about Si solution in the early 3d transition-metal tri-aluminides and the corresponding effects on their stability and structural properties.

There have been efforts on Si solution in the Al_3T phases [38-42, 39] along with the intensive study on the binary phases [4-8,10,26-30, 40, 41]. Recently, Dumbre *et al.* studied the impact of thermal treatments on formation of $(\text{L}_{12}\text{-})(\text{Al},\text{Si})_3\text{Sc}$ in Al-Si-Sc alloys [43]. Yao performed first-principles calculations on the elastic and electronic properties of $\text{L}_{12}\text{-}(\text{Al},\text{Si})_3\text{Sc}$ phase [44]. Using first-principles density functional theory approach, Castillo-Sánchez *et al.* investigated Si substitution in the $\text{Al}_3(\text{Zr},\text{Ti})$ intermetallic compounds with the D_{022} - and D_{023} -type structures [39]. Meanwhile, there is still a lack of comprehensive understanding about the Si solution in the early 3d transition metal tri-aluminides phases.

Formatted: Font: Italic

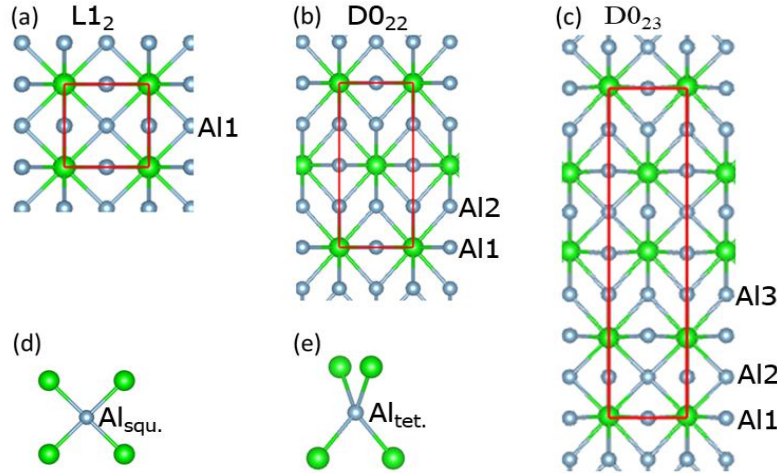


Figure 1. Schematic structures of the **ebbie**-L1₂- (a), D0₂₂- (b) and D0₂₃-TAI₃ (c) projected along the [100] orientations, and local coordination of Al atom in a square-planar (d) and tetrahedral (e) coordination by four T atoms. The red-lines means the *b*-axis (horizontal) and *c*-axis (vertical) in (a), (b) and (c). The *z*-component of the unit cell for D0₂₃-TAI₃ has been shifted by 1/8, which sets the Al atoms at the Wyckoff 4e sites atoms at *z* = 0. The larger green spheres represent Ti and smaller silvery Al.

Here we investigate Si solution in the Al₃T (T = Sc, Ti and V) forms of L1₂-, D0₂₂- and D0₂₃-type structures in a systematic way using a first-principles density-functional theory method. This study reveals that Si solution favors the Al sites in Ti square-planar coordination (Figure 1d) and stabilizes the D0₂₂-Al₃Ti phase so that the D0₂₂-(Al_{1-x}Si_x)₃Ti phases become more stable than the binary ground state (D0₂₃-Al₃Ti) phase. The Si solution in D0₂₂-Al₃V occurs only at elevated temperatures. The obtained information here helps not only understand the phase relationships and the rich variety of experimental results in the literature, but also design new Al alloys of desirable mechanical and chemical properties based on Al scrap/waste parts, which benefits develop our circular society in an environmental-friendly sustainable way.

2. Details of computations

To assess the relative stability of the binary Al₃T compounds, the energy difference between the investigated X-Al₃T and the corresponding cubic L1₂-phase is defined as:

$$\Delta E_1 = E(X\text{-Al}_3\text{T}) - E(\text{L1}_2\text{-Al}_3\text{T}) \quad (1)$$

Here, $E(X\text{-Al}_3\text{T})$ and $E(\text{L1}_2\text{-Al}_3\text{T})$ represent the calculated total valence-electron energies for the related X-phase and related L1₂-Al₃T phase, respectively.

For dilute solution of **Si** and the early 3d transition metals in the Al matrix, the solution energy is defined as:

$$\Delta E(\text{FM}^*) = E(\text{Al}_{n-1}\text{FM}) - [(n-1)/n] \times E(\text{Al}_n) + E(\text{FM}) \quad (2)$$

Where, $E(\text{Al}_{n-1}\text{FM})$, $E(\text{Al}_n)$, $E(\text{FM})$ represent respectively, the calculated energies for the substituted Al_{n-1}FM, Al_n and the elemental solid FM. The calculated total valence-electron energy of the same supercell of Al_n ($n=108$ in a $3a_0 \times 3a_0 \times 3a_0$, a_0 is the lattice parameter of the Al cell) is used for systematic error cancellation. The unit of the solution energy is eV per FM.

For a ternary Si doped (Al_{1-x}Si_x)₃T phase, the formation energy with respect to the elemental solids Si, Al and dilute solution of T in the Al matrix is defined as,

$$\Delta E_f = E[(\text{Al}_{1-x}\text{Si}_x)_3\text{T}] - \{3(1-x)E(\text{Al}) + 3xE(\text{Si}) + E(\text{T}^*)\} \quad (3)$$

Here $E[(\text{Al}_{1-x}\text{Si}_x)_3\text{T}]$, $E(\text{Al})$, $E(\text{Si})$ and $E(\text{T}^*)$ represent respectively, the calculated total valence-electron energies for the (Al_{1-x}Si_x)₃T phase, the elemental solids Al and Si, and a-the dilute solution of a 3d transition metal, T in the Al matrix (T*) in Equation 2, respectively.

The unit for both Equations 1 and 3 is eV/f.u. (f.u. represents formula unit, (Al_{1-x}Si_x)₃T). A negative ΔE_1 value in Equation 1 means that the X-Al₃T is more stable than the L1₂-phase. For Equation 3, a negative value

of the formation energy means favoring formation of the $(\text{Al}_{1-x}\text{Si}_x)_3\text{T}$ phase with respect to the elemental solids, Al, Si and T*. At $T = 0$ K and $P = 0$ Pa, the calculated formation energy in Equations 2 and 3 is equal to the related reaction enthalpy when the zero-vibration contribution is ignored.

A $3a_0 \times 3a_0 \times 3a_0$ (a_0 is the lattice parameter of the cubic Al unit cell) supercell which contains 108 Al atoms is employed to model the dilute solution of Si and an early 3d transition metal in the Al matrix. $2a_0 \times 2a_0 \times 2a_0$ ($3a_0 \times 3a_0 \times 3a_0$), $2a_0 \times 2a_0 \times 1c_0$ and $2a_0 \times 2a_0 \times 1c_0$ (a_0 and a_0 are the lattice parameters of the conventional cells for the corresponding structures) supercells are employed-used for the cubic $L1_2$ -, tetragonal $D0_{22}$ - and $D0_{23}$ - Al_3T phases and they-These supercells contain 32(108), 32, and 64 atoms, respectively. The large supercell $3a_0 \times 3a_0 \times 3a_0$ for the $L1_2$ -phase was employed-utilized to justify the usage of the smaller supercells.

A plane-wave approach embedded in the first-principles package VASP (Vienna *Ab initio* Simulation Package) [45] has been employed in the present study. The Generalized Gradient Approximation (GGA) [46] within the projector-augmented wave frame [47] has been used for the correlation and exchange terms. This is because that the GGA works better than the Local Density Approximations (LDA) for transition metals and their compounds [46,48,49]. Cut-off energies are reasonably high ($E_{\text{CUT}}/E_{\text{AUG}} = 400.0$ eV/550.0 eV) as compared with the default values of the atoms ($E_{\text{MAX}}/E_{\text{AUG}} = 245.3$ eV/322.1 eV for Si, 180.2 eV/240.3 eV for Al, 116.1 eV/154.8 eV for Sc, 133.7 eV/178.3 eV for Ti, and 144.4 eV/192.5 eV for V, respectively). Dense k -meshes for the structural optimizations and total energy calculations are employed-used, e.g. a $10 \times 10 \times 10$ mesh with k -points ranging from 35(75) to 250(500) for the $L1_2$ - and $(D0_{22})\text{-Al}_3\text{T}$ supercells, and a $10 \times 10 \times 6$ mesh with k -points ranging from 45 to 300 for $D0_{23}\text{-Al}_3\text{T}$ supercells, depending on the symmetry in the Brillouin Zone for the based on the Monkhorst-Pack scheme [50]. Test calculations for the cut-off energies and k -meshes provided that the present settings are reasonable with energy deviations being less than 1meV/atom.

Formatted: Font: Italic

3. Results and Discussion

3.1. Calculated results for the elemental solids and dilute solutions

First, structural optimizations were performed for the elemental solids, α -Al with the face-centred cubic structure and Si with the diamond-type structure, as well as the early 3d transition metals [3,26]. Both Sc and Ti have simple hexagonal lattices, while V has a body-centred cubic structure [3]. We also performed calculations for dilute solution of the early 3d transition metals in bulk-Al. The obtained results are listed in Table 4. The available experimental data in the literature are included for comparison.

Table 4. The calculated results (lattice parameters, formation energies and important interatomic distances) for the elemental solids, Al, Si, Sc, Ti and V, and the dilute solution of Si and the early 3d transition metals in the Al matrix. The solution energy, $\Delta E(\text{FM}^*)$ is obtained according to Equation 2. The electronic configurations for the elements are listed in which the element labels in the square parenthesis represents the core electrons. $\Delta = (d_{\text{calc}} - d_{\text{exp}})/d_{\text{exp}} \times 100$ represents the deviations of the computed lattice parameters (d_{calc}) from the corresponding experimental values extended to 0 K (d_{exp}) in [3] in the parenthesis. BCC represents body-centred cubic.

Element /ele.config.	Symmetry	Latt. para. (Å) and (Δ) (exp. data at 0 K [3])	Interatomic Distances (Å) and coordination-type
Al [Ne]3s ² 3p ¹	Cubic Fm-3m (nr. 225)	$a = 4.039(0.2 \%)$ (4.0325)	Al-Al: 2.86($\times 12$) (cuboctahedral)
Si [Ne]3s ² 3p ²	Cubic Fd-3m (nr. 227)	$a = 5.468(+0.7 \%)$ (5.42982)	Si-Si: 2.37($\times 4$) (tetrahedral)
Sc [Ar]4s ² 4p ⁰ 3d ¹	Hexagonal P6 ₃ /mmc (nr. 194)	$a = 3.320(+0.5 \%)$ (3.3035) $c = 5.157(-1.9 \%)$ (5.2552)	Sc-Sc: 3.21($\times 6$), 3.32($\times 6$) (distorted antibuboctahedral)
Ti [Ar]4s ² 4p ⁰ 3d ²	Hexagonal P6 ₃ /mmc (nr. 194)	$a = 2.929(-0.5 \%)$ (2.9451) $c = 4.593(-1.8 \%)$ (4.6783)	Ti-Ti: 2.85($\times 6$), 2.93($\times 6$) (distorted antibuboctahedral)
V [Ar]4s ² 4p ⁰ 3d ³	BCC, Im-3m (nr. 229)	$a = 2.978(-1.5 \%)$ (3.0223)	V-V: 2.58($\times 8$) (cubic)
Dilute solution of impurities in Al matrix (see Equation 2)			
Al₁₀₇FAl₁₀₇M	Local symmetry	$\Delta E(\text{FM}^*)$	T-Al bonds (Å)
Sc*	O_hO_h	-1.04 eV/Sc	Sc - Al: 2.90($\times 12$)
Ti*	O_hO_h	-1.18 eV/Ti	Ti - Al: 2.83($\times 12$)
V*	O_hO_h	-0.57 eV/V	V - Al: 2.78($\times 12$)
Si*	O_hO_h	+0.43 eV/Si	Si -Al: 2.84($\times 12$)

Formatted: Subscript

The calculations reproduced the experimental values well for the simple s-p elements, Al and Si with deviations within 1 %. Meanwhile for the early 3d transition metals, the calculated lattice parameters deviate somewhat larger, 1.5 % for the cubic V and about 1.8 %/1.9 % for the c-axis of the hexagonal lattices for Sc/Ti, respectively from the experimental values in the literature [3]. The calculated local Al-T bond-lengths in the dilute solutions decreases with increasement of valence electrons in the order, Sc, Ti and V, which is in line with the atomic radii in the pure metals (Table 4I). The calculated solution energies for the early 3d transition metals in the Al matrix are negative, indicating solution in Al matrix are favored with respect to the elemental solids. Meanwhile, Si solution in Al is not favored with a notable formation energy of 0.43 eV/Si which agrees with the previous calculations using the same approach [37,48]. The calculated Si-Al interatomic distance is 2.84 Å, which is slightly shorter than that of the Al-Al bonds. This result indicates that Si prefers being bulk rather than solution not dissolving in the Al lattice. Thus, the energy of bulk Si is used as a reference to assess the stability of the compounds in equilibrium.

3.2. Binary Al₃T phases

Structural optimizations and total-energy calculations were carried out for the binary Al₃T phases. We also calculated the formation energies for the related D0₁₉-Al₃T structure [26,27]. The calculations showed that the D0₁₉-Al₃T phases are notably less stable with the calculated energies being over 4.0 eV/f.u. higher than those of the corresponding L1₂-Phases. Thus, the results for the D0₁₉-Al₃T phases are not discussed in the present paper. The calculated results for the L1₂-, D0₂₂- and D0₂₃-phases are listed in Table 2II. The experimental values available in the literature are included in parenthesis for comparison.

Table 2II. The calculated results (lattice parameters, formation energies and intermetallic bonds) in the binary TAl₃ (T = Sc, Ti, V) phases. The energy difference, ΔE_f are obtained via Equation 1. The experimental lattice parameters available in the literature are included in parenthesis together with the references. Here, fu represents TAl₃ formula unit. The most stable phases are marked in *italic-bold*.

Phase	Latt. / Spacegroup	Latt. paras (Å), vol.(Å ³ /f.u.), ΔE_f (eV/f.u.)			Remarks
		Al ₃ Sc	Al ₃ Ti	Al ₃ V	
					T are in Al cuboctahedral coordination.
L1 ₂	Cubic Pm-3m (nr. 221)	$a = 4.103$ (4.106[8]) (4.105[51]) $V = 69.20$ $\Delta E_f = \mathbf{0.0}$	$a = 3.977$ (3.967[50]) (-) $V = 62.91$ $\Delta E_f = 0.0$	$a = 3.897$ (-) (-) $V = 59.19$ $\Delta E_f = 0.0$	Al is coordinated in T square-planar coordination (Fig. 1d).
D0 ₂₂	Tetragonal I4/mmm (nr. 139)	$a = 4.021$ (-) (-) $c = 8.805$ (-) (-) $V = 71.17$ $\Delta E_f = +0.364$	$a = 3.841$ (3.836 to 3.854 [27]) (3.849 [34]) $c = 8.618$ (8.584 to 8.612[27]*) (8.610[34]) $V = 63.57$ $\Delta E_f = -$ 0.018 108	$a = 3.765$ (3.722[36]) (3.779[52]) $c = 8.307$ (8.195[36])* (-) (8.322[52])* $V = 58.86$ $\Delta E_f = -\mathbf{0.541}$	Two types of Al Al1 at 2b in T square-planar coordination (Fig.1d) Al2 at 4d in T tetrahedra coordination (Fig.1e) *The experimental D0 ₂₂ -Al ₃ Ti/Al ₃ V samples prepared with different chemical compositions.
D0 ₂₃	Tetragonal I4/mmm (nr. 139)	$a = 4.039$ (-) (-) $c = 17.218$ (-) (-) $V = 70.23$ $\Delta E_f = +0.184$	$a = 3.895$ (3.875 to 3.947[27]) $c = 16.662$ (16.679 to 16.926[27]*) $V = 63.19$ $\Delta E_f = -\mathbf{0.131}$	$a = 3.806$ (-) (-) $c = 16.315$ (-) (-) $V = 59.08$ $\Delta E_f = -0.268$	There three types of Al Al1 at 4e and Al2 at 4c are in distorted square-planar coordination by T with Al out of the Ti plane. Al3 at 4d are in distorted tetrahedra coordination.

As shown in Table 2II, the present calculations produced the following conclusions results.

1). With increasing the number of d electrons in the transition metal, L1₂-Al₃Sc, D0₂₃-Al₃Ti and D0₂₂-Al₃V are the ground state phases with formation energies notably lower than the rests of the corresponding phases. D0₂₃-Al₃Ti has a formation energy being 0. ~~11~~**02** eV/f.u. lower than its D0₂₂-phase. This conclusion agrees with the previous works [27-29].

2). The calculated lattice parameter of $L1_2\text{-Al}_3\text{Sc}$ is close to the experimental values from different groups [8,51]. Meanwhile, the experimental values for the ground state $D0_{22}\text{-Al}_3\text{V}$ differ notably from each other [36,52]. The calculated lattice parameters are in-between ~~the range~~ those of the available experimental data (Table 2II).

3). As summarized in the references [27,52], the experimental lattice parameters for both $D0_{22}$ - and $D0_{23}\text{-Al}_3\text{Ti}$ phases in the literature vary in ranges within 2 %. The calculated values are close to the experimental values.

Intrinsic defects in the Al_3T phases have been investigated. There are high energy costs for Al substitutions of T in the ground state Al_3T phases ($L1_2\text{-Al}_3\text{Sc}$, $D0_{23}\text{-Al}_3\text{Ti}$ and $D0_{22}\text{-Al}_3\text{V}$). For example, it costs over 0.70 eV to replace one T by Al with respect to T solution in the Al matrix. ~~This indicates that this type of defect is very unlikely.~~ The calculations also produced high energy costs to produce Al vacancies, e.g. it costs 0.81 eV to create one Al vacancy in the $L1_2\text{-Al}_3\text{Ti}$ phase. ~~The calculations indicating indicate unlikelihood for the intrinsic defects to occur.~~ Therefore, we limit ourselves to Si ~~solutions-dissolving~~ at the Al sites in the compounds.

3.3 Effects of Si solution on stability of the Al_3T phases

The study includes various configurations of Si solutions at the Al sites in the Al_3T phases. It showed that the Si atoms prefer uniform layer-resolved distributions in the structures. For example, for two Si doped at the Al1 sites in the $D0_{23}\text{-Al}_3\text{Ti}$ supercell there are four equal layers, $z = 0.0, 1/4, 1/2$ and $3/4$ (Figure 1c). The calculations showed that the formation energies for the configuration with two Si at the same layer ($z = 0.0$) and that with two Si at the nearby layers ($z = 0.0$ and 0.25) are, respectively about 0.04 eV and 0.02 eV higher than that with the Si atoms uniformly distributed (Si1 at $z = 0.0$ and Si2 at $z = 0.50$). ~~This phenomenon may originate from the size effect that the Al-Si bond length (2.84 Å) is shorter than that of Al-Al (2.86 Å, Table 1) and the chemical repulsion between the charged Si ions.~~ This helps us choose configurations of high stability. The results for ~~the~~ Si solutions at the Al sites in the Al_3T phases are addressed separately in the following subsections.

3.3.1 Si solution in Al_3Sc

Figure 2 shows the calculated formation energies for the highly stable configurations with Si solutions in the Al_3Sc phases. Clearly, Si solution in $L1_2\text{-Al}_3\text{Sc}$ cost a notable amount of energy. Doping one Si at the Al site costs 0.28 eV, indicating that it is highly unlikely to occur at low temperature. However, at high temperature, kinetic factor enables dope a moderate amount of Si at the Al sites, which agrees with experimental assumptions [43].

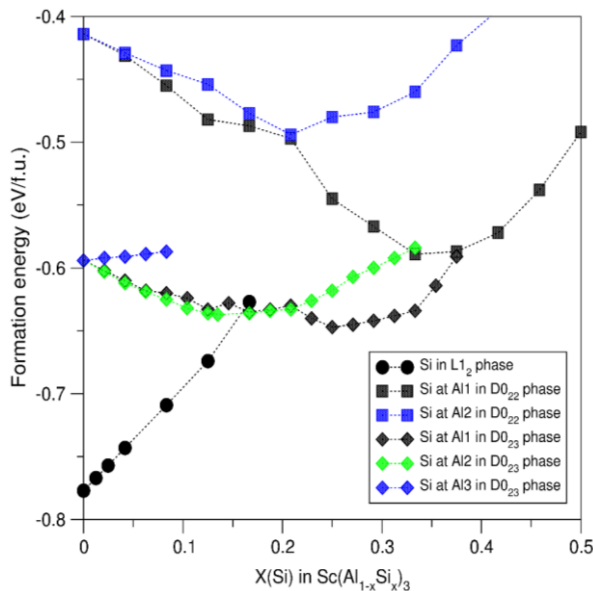


Figure 2. The dependences of the formation energies on Si content in the Al₃Sc phases. Clearly, the binary L1₂-Al₃Sc is the most stable phase in the system.

Si solution at the Al sites in D0₂₂-Al₃Sc phases is favored. With increasing Si content, the configurations become more stable. The most stable configuration is the full Si occupation of the Al1 site, which has the chemical formula, D0₂₂-Al₂SiSc. This configuration gains a notable amount of energy (about 0.17 eV/f.u.). However, such an energy gain is not enough to make this phase more stable than L1₂-Al₃Sc. Addition of extra Si at the Al2 sites gradually reduces the stability of D0₂₂-Al₂SiSc.

For the D0₂₃-phase, Si prefers the Al1 and Al2 sites where Al atoms are in distorted Ti square-planar coordination, meanwhile Si solution at the Al3 sites with distorted Ti tetrahedral coordination costs moderate energies. The most stable configuration has the chemical formula, D0₂₃-(Al_{0.708}Si_{0.292})₃Sc. This formation energy is still much higher than the binary cubic L1₂-phase as shown in Figure 2.

Overall, the calculations revealed preferences of Si solution in D0₂₂- and D0₂₃-Al₃Sc. The Si stabilization, however, is not strong enough to overtake the ground state L1₂-Al₃Sc phase. This study elucidates the experimental observations that this cubic phase exists and has been observed in the Al alloys. Moreover, the measured lattice parameters of L1₂-Al₃Sc in the Al alloys of different Si contents are close to each other [8,43,51], indicating minor Si content.

3.3.2. Si solution stabilizes D0₂₂-Al₃Ti

The calculations revealed that Si solution in L1₂-Al₃Ti is not favored with an energy cost of 0.43 eV to replace one Al by Si. Such energy cost is the close to that to dope one Si in bulk Al (Table 4), indicating highly impossible to occur.

Doping one Si atom at both Al1 and Al2 sites costs 0.16 eV and at the Al3 sites 0.28 eV in the D0₂₃-phase, respectively. The Si doping at the Al1 sites is shown in Figure 3. The formation energy increases almost linearly with the Si content in the D0₂₃-phase.

Si solution at both Al1 and Al2 sites in D0₂₂-Al₃Ti is favored. The formation energy for one Si at the Al1 sites is about -0.05 eV lower than that at the Al2 sites, indicating the former is preferred over the latter. The trends of relationships between the formation energies and Si content for Si solutions at the Al1 and the Al2 sites are shown in Figure 3. The formation energy decreases with increase of Si content and reach minima at $x(\text{Si}) = 1/6$ in (Al_{1-x}Si_x)₃Ti. It then increases with further addition of Si. Thus, the most stable configurations have chemical composition, D0₂₂-(Al_{0.833}Si_{0.167})₃Ti with Si at Al1. Analysis showed that the most stable configuration of the composition, the Si atoms are distributed away from each other, in a uniform way. This Si content composition is notably lower than that in the reported D0₂₂-(Al_{2/3}Si_{1/3})₃Ti with the Si full occupation of the 2b (Al1) sites, which configuration has the minimum enthalpy in the Al₃Ti-Si₃Ti system in the recent publication (Figure 12 in [39]).

Figure 3 revealed that the formation energies for the configurations with over 2 at.% Si at the Al1 sites in the D0₂₂-phase are lower than that of the ground state D0₂₃-Al₃Ti phase. This indicates that the Si doped D0₂₂-phase replaces the binary D0₂₃-Al₃Ti phase to be the ground state.

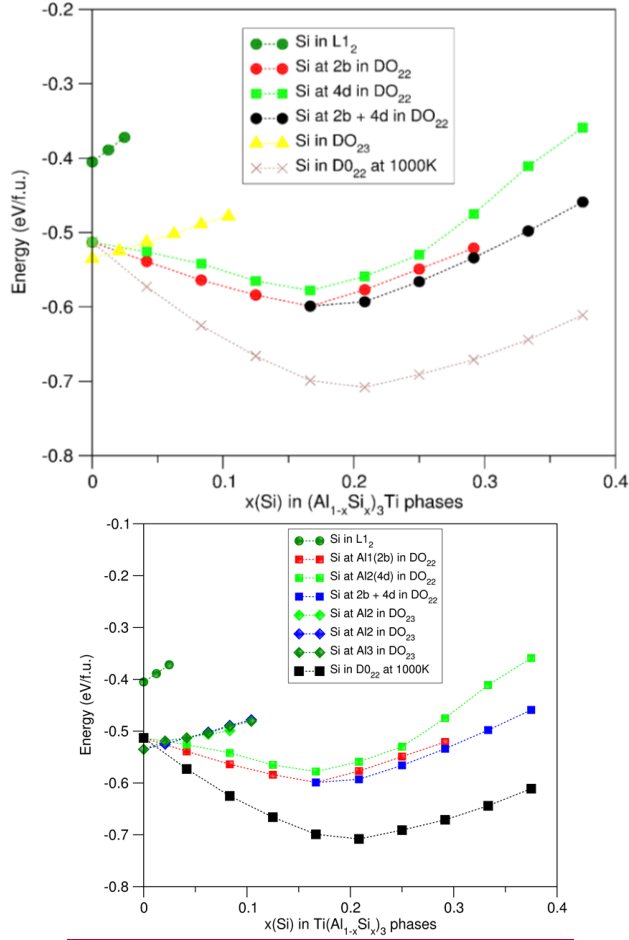


Figure 3. Relationships between the formation energies and Si content in the $(Al_{1-x}Si_x)_3Ti$ phases. Clearly, Si solution stabilizes the DO_{22} -phase that it overtakes the DO_{23} - Al_3Ti phase as the ground state.

The partial occupation of Si at the Al sites indicates the **determinant important** role of configurational entropy contributions in the stability at elevated temperature. The stability of the Si doped DO_{22} -phase at the casting temperature can be estimated via the Gibbs energy, $\Delta G = \Delta H - T\Delta S_{conf}$, where ΔH is the formation enthalpy being equal to ΔE_f at 0 K and 0 Pa, when the zero-point vibration contribution is ignored, T is the temperature, the configurational entropy, $\Delta S_{conf} = R \ln W$ (R is the Boltzmann constant and W the number of configurations in the random model, **considering kinetic factor over the moderate energy hierarchy ($<0.05eV/f.u.$) at such high temperature**). The obtained values for the Gibbs energies at 1000 K are plotted in Figure 3.

Figure 3 shows a shallow potential valley for the Gibbs energy on Si in the range $x = 0.17$ to 0.25 in the formula $DO_{22}-(Al_{1-x}Si_x)_3Ti$ at the casting temperature with the minimum at $x = 0.208$. This indicates dependence of Si content in the obtained samples on the local chemical composition and thermal treatments.

In brief, Si solution is favored in DO_{22} - Al_3Ti . The partial occupation of Si at the Al sites also indicates dependence **of Si content in the samples** on **the chemical composition and** preparation conditions. With a moderate Si content (2 at%Si), the DO_{22} -phase overtakes the DO_{23} -phase as the ground phase. This study provides explanation about the long-standing puzzle that the Al_3Ti particles observed in most Al-alloys have the

D0₂₂-type structure [33-35], whereas the theoretical calculations predicted that the D0₂₃-Al₃Ti is the ground state in the Al-Ti system [27,30].

3.3.3. Si solution in Al₃V

Figure 4 shows the calculated relationships between the formation energies and Si contents at the Al sites in the Al₃V phases. There are rather simple relations between the formation energies and the Si solution at the Al sites for the Al₃V phases that it costs energies for Si solution in any of the phases. Thus, there is no change of the phase relations due to Si solution (Figure 4) and the D0₂₂-phase remains the ground state.

Interestingly, the formation energies for Si solution at the Al1 sites are lower than the corresponding one at the Al2 sites in D0₂₂-Al₃V. This is opposite to the cases in D0₂₂-Al₃Sc and Al₃Ti.

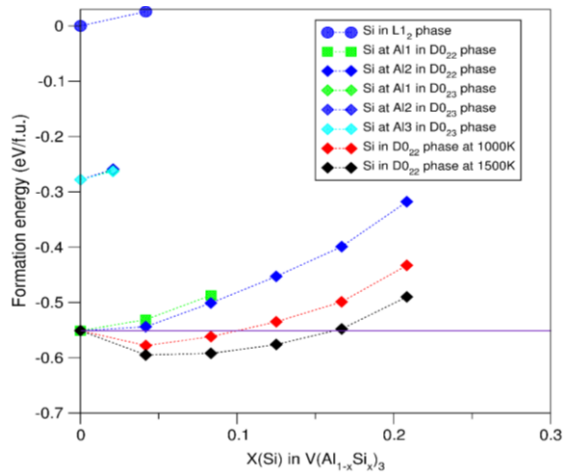


Figure 4. Relationships between the calculated formation energies and Si contents for the Al₃V phases. Clearly, Si solution in the phases is not favored with moderate costs for Si solution in D0₂₂-Al₃V. The Si solution occurs at elevated temperatures due to thermodynamic contribution.

Figure 4 shows that for D0₂₂-Al₃V the costs for Si solution in this phase are moderate. It is reasonable to consider its stability at elevated temperatures. Configurational entropy contributions were estimated for Si solutions at the Al sites in D0₂₂-Al₃V using the same approach in subsection 3.3.2. The obtained data for the Gibbs energies at 1000 K (about the casting temperature) and 1500 K (around the formation temperature of Al₃V phase [6]) were plotted into Figure 4.

The Si regions of negative Gibbs energy of the system are about 11 at.% at 1000K and 17 at.% at 1500 K, respectively. Therefore, D0₂₂-(Al,Si)₃V may be formed and stable at elevated temperatures.

Overall, the Si solution in Al₃V is not favored. Meanwhile, energy costs for Si solution in D0₂₂-(Al,Si)₃V are moderate, indicating occurrence of Si solution at high temperatures. Naturally, the Si content in a prepared sample depends on the chemical composition and the experimental conditions.

3.4 Crystal chemistry of the (Al_{1-x}Si_x)₃T phases

3.4.1 Structural properties of the highly stable (Si-doped) Al₃T phases

The present first-principles calculations showed a rich variety of Si stabilization effects in Al₃T phases. The binary cubic L1₂-Al₃Sc is the ground state and Si solution in this phase is energetically costly. Thus, Si content in L1₂-Al₃Sc is moderate even at elevated temperatures. Meanwhile, Si solution at the Al sites in D0₂₂-Al₃Ti is favored. Si solution in D0₂₂-Al₃V costs only moderate energies and thus, occurs at elevated temperatures. Therefore, it is likely to obtain D0₂₂-(Al_{1-x}Si_x)₃V samples via e.g. quenching approaches. The influences of Si content in the D0₂₂-(Al_{1-x}Si_x)₃T (T = Ti, V) on their crystal structures become important for characterizing the phase in Al alloys. The relationships between the lattice parameters and Si contents for the D0₂₂-Al₃T (T = Ti and V) are presented in Figure 5.

As shown in Figure 5, the lattice parameters and the corresponding volumes for both D0₂₂-Al₃T (T = Ti and V) systems decrease with increasing Si content in common. This general trend is in line with the smaller atomic

radius for Si (1.15 Å) than that of Al (1.43 Å) [53] and with the calculations that the shorter Al-Si bonds for the dilute Si solute in Al (1.84 Å) than that of the Al-Al bonds (1.86 Å) (Table I).

Figure 5a shows that for $D0_{22}-(Al_{1-x}Si_x)_3Ti$, the length of the a -axis for the configurations with Si at Al2 decreases more rapidly than that for those with Si at the Al1 (2b) sites. Opposite behavior was uncovered for the c -axis which length decreases quicker for Si at the Al2 (4d) sites. The volume of the configurations with Si at Al1 decreases faster as well.

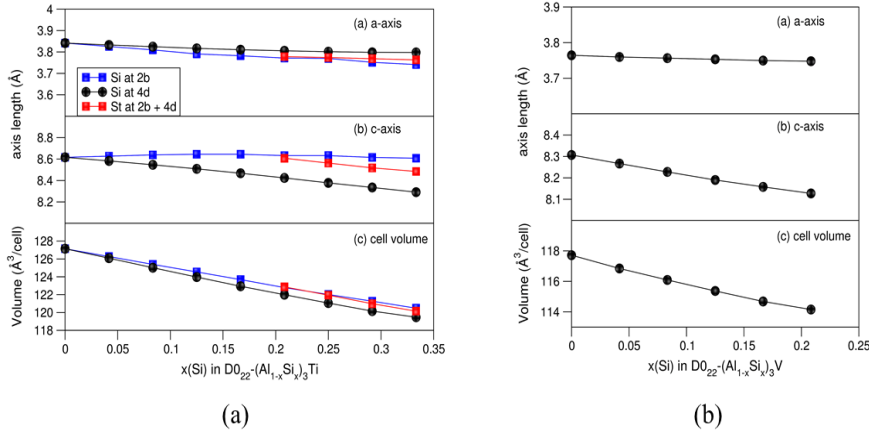


Figure 5. Dependences of lattice parameters and cell volumes on Si content at the Al1 and Al2 sites in $D0_{22}-(Al_{1-x}Si_x)_3Ti$ (a), and at the Al2 sites in $D0_{22}-(Al_{1-x}Si_x)_3V$ (b). Clearly lengths of the lattice parameters and the cell volumes decrease with increasing Si content.

The lattice parameters for the most stable configuration, $D0_{22}-(Al_{0.833}Si_{0.167})_3Ti$ with Si at the Al1 (Wyckoff 2b) sites are $a = 3.810$ Å and $c = 8.468$ Å, which are about 5.2 % and 3.8 %, respectively smaller than those of $D0_{22}-Al_3Ti$ (Table 2II). Figure 3 shows that at 1000 K the Gibbs energies are moderate in the range of Si contents (x) from 0.125 to 0.333, in which the a -/ c -axis have lengths between 3.79 Å/8.64 Å to 3.74 Å/8.61 Å for Si at the Al1 sites and 3.82 Å/8.52 Å to 3.80 Å/8.2 Å for Si at the Al2 sites (Figure 5), respectively. This helps understand the rich variation of the lattice parameters from the experiments [27,33-35].

The Si solution in $D0_{22}-Al_3V$ is possible at elevated temperatures (Figure 4). The lattice parameters (a/c) decrease moderately from 3.764 Å/8.307 Å ($x(Si) = 0$) to 3.756 Å/8.227 Å ($x(Si) = 8.3$ %). The observation large range of the lattice parameters (Table 2II) in the experiments [36,51] may come from a different origins.

3.4.2 Electronic properties of and chemical bonding in the stable $(Al_{1-x}Si_x)_3T$ phases

Electronic band structure calculations were worked out for the highly stable $L1_2-Al_3Sc$, $D0_{22}-(Al_{0.833}Si_{0.167})_3Ti$ and $D0_{22}-Al_3V$ and meta stable $D0_{22}-(Al_{0.958}Si_{0.042})_3V$. The obtained local coordination of Sc by Al atoms in the $L1_2-Al_3Sc$ is shown in Figure 6a, while the electron density distributions in the rest of the above-mentioned phases are shown in Figures 6b to 6d. The curves of the related densities of states for $D0_{22}-(Al_{0.833}Si_{0.167})_3Ti$ and $D0_{22}-Al_3V$ and $D0_{22}-(Al_{0.958}Si_{0.042})_3V$ are shown in Figure 7, whereas the DOS curves for $L1_2-Al_3Sc$ and novel $D0_{22}-Al_3Ti$ are shown in Figure 8a and 8b respectively, with the latter for comparison.

The euboctahedroncuboctahedral-eordinated-coordination of Sc by Al in $L1_2-Al_3Sc$ is shown clearly in Figure 6a. Symmetries and the overlapping between the electron densities in the Al-V-Al chains in $D0_{22}-Al_3V$ in the a - b plane are presented in Figure 6b. Figure 6c also shows the overlapping of electron clouds of Si with those of V, indicating local strong Si-V bonding. For $D0_{22}-(Al_{0.833}Ti_{0.167})_3Ti$, there are electron overlapping in the Ti-Si-Ti chains parallel to the b -axis, indicating chemical bonding between Ti and Si (Figure 6d).

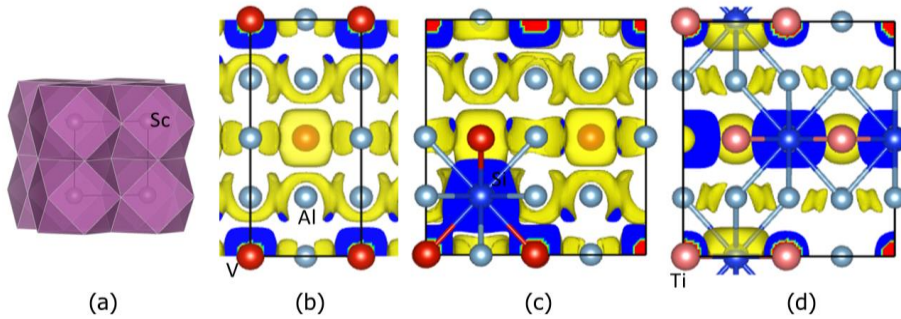


Figure 6. Schematic coordination and electron density distributions in $L1_2$ - Al_3Sc (a), $D0_{22}$ - Al_3V (b), $D0_{22}$ - $(Al_{0.958}Si_{0.042})_3V$ (c) and $D0_{22}$ - $(Al_{0.833}Si_{0.167})_3Ti$ (d) along (approximately for a) the $[100]$ orientation. The black lines represent the b -axis (horizontal) and c -axis (vertical). The bonds between Si and T/Al are shown for the Si doped systems (c) and (d).

The curves of the calculated partial density of states for the Al and Sc atoms in and the total density of states of $L1_2$ - Al_3Sc is shown in Figure 8a. The frame of the present calculations-calculated results agrees with the previous calculations by Duan et al. who employed the first-principles density functional theory within the local-density approximation [54]. The Al 3s states dominates the lower part of the valance band (-10.0 eV to -3.0 eV) (figure Figure 8a) while the DOS curve around the Fermi level is dominated by Sc 3d states mixed with Al 3p states (from -3.0 eV to the Fermi level, zero eV). There is a broad valley ranging from -0.9 eV to +0.5 eV in which the Fermi level falls. Such low DOS at the Fermi level indicates electronic stability of this crystal according to Stoner's theory [55]. This agrees with the energy cost for Si solution.

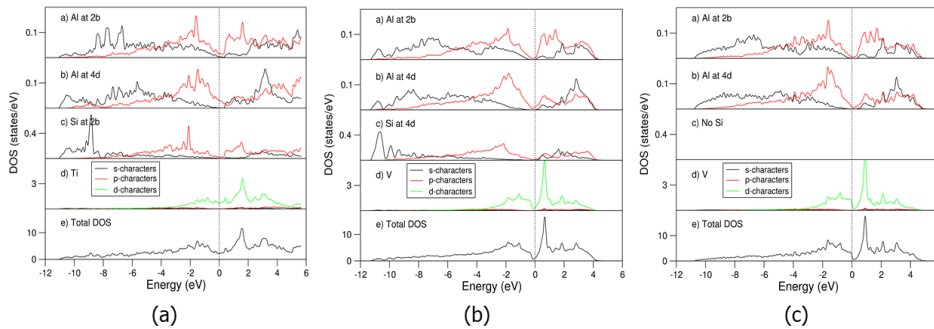


Figure 7. Partial density of states of selected atoms (pDOS) in and total density of states (tDOS) of the highly stable $D0_{22}$ - $(Al_{0.833}Si_{0.167})_3Ti$ (a), $D0_{22}$ - Al_3V (c) and $D0_{22}$ - $(Al_{0.958}Si_{0.042})_3V$ (b). The unit is states/eV per atom for the pDOS curves and states/eV per primitive unit cell for the tDOS curves. The vertical dotted lines at zero eV represent the Fermi level.

Figure 7c shown the DOS curves for $D0_{22}$ - Al_3V . The DOS curves can be divided into a valence band (from -10.7 eV to 0.0 eV) and the conduction band above the Fermi level above with a pseudo-gap in-between. The lower part of the valence band (from the bottom to -3.0 eV) is dominated by Al 3s states while the upper part (-3.0 eV to 0.0 eV) is dominated by V 3d and Al 3p states. The Fermi level is just at the starting of the valley which is determined by the V 3d states.

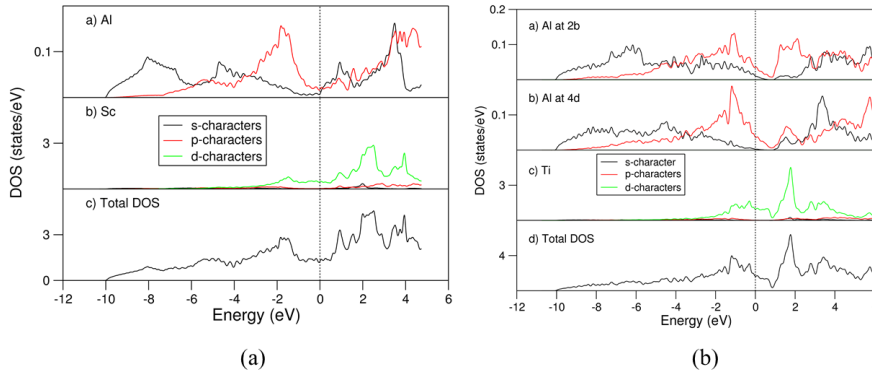


Figure 8. pDOS and tDOS of L1₂-Al₃Sc (a) and novel D0₂₂-Al₃Ti (b). The unit is states/eV per atom for the pDOS curves and states/eV per primitive unit cell for the tDOS curves. The vertical dotted lines at zero eV represent the Fermi level.

The overall shapes of the DOS curves for the Si doped, D0₂₂-(Al_{0.958}Si_{0.042})₃V (Figure 7b) are similar with to the corresponding binary Al₃V (Figure 7c). A close look reveals differences. First addition of Si causes lowering of the valence band to -11.3 eV. This is due to mixing of the Si 3s states which dominated the lower part of the valence band from -11.3 eV to -8.0 eV together with the Al 3s states. Secondly, the Fermi level shifts from the start of the DOS valley to its middle (Figure 7b) from the beginning of the DOS curve in the parent binary (Figure 7c). The higher DOS at the parent D0₂₂-Al₃V (Figure 7c) might be the cause of moderate Si solution at the Al sites, which may shift the Fermi level to the middle of the DOS valley dominated by V 3d states to enhance the stability of the compound.

The frames overall shapes of the DOS curves of D0₂₂-(Al_{0.833}Si_{0.167})₃Ti (Figure 7a) are also similar with to the corresponding ones of D0₂₂-(Al_{0.958}Si_{0.042})₃V (Figure 7b). Meanwhile some subtle differences can be recognized: a) the Si 3s states form show more localized between the bottom to -8.0 eV in the valence band in the former as compared to those in the latter; b) The sum of the occupied Ti 3d states in Figure 7a is notably smaller than that in Figure 7b, indicating more 3d electron in V and in Ti. Moreover, the tDOS curve around the Fermi level in D0₂₂-(Al_{0.833}Si_{0.167})₃Ti is dominated by Ti 3d state and form a plateau with electron density of states at Fermi level being 0.71 states/eV for Ti 3d states. In comparison the total DOS curve of the binary D0₂₂-Al₃Ti has a deep valley at 0.86 eV (See Figure 8b). Using rigid band filling model, we may conclude that replacement of Al by Si adds electrons into the system, shifts the Fermi level at a high density of the binary compound (Figure 8b) to in the DOS valley at a higher energy (Figure 7a), which enhances the stability of the system according to the criteria [55]. This is the physics behind the stability effect of Si solution in D0₂₂-Al₃Ti.

3.5 Electron count and the (Al_{1-x}Si_x)₃T phases

The early 3d transition metals belong to the s-d elements with electronic configurations: Sc [Ar] 3d¹ 4s², Ti [Ar] 3d² 4s², and V [Ar] 3d³ 4s², here [Ar] represents the close-shell core electrons. Our calculations showed a trend between the electron number and the energetic hierarchy of the phases: by increasing electron number, the preferred structure is L1₂ for ScAl₃ to D0₂₃ for TiAl₃, and to D0₂₂ for VAl₃. Analogous behavior is expected for the related TAl₃ compounds with T = the early 4d/5d transition metals (Y/Lu; Zr/Hf and Nb/Ta) [39, 43, 52, 56]. Such an energetic hierarchy and phase relations have been confirmed by our systematic first-principles calculations for the TAl₃ family (Table III) with the same code and settings described in Section 2.

Table III Calculated formation energies (ΔE_f) for the TAl₃ (T = Sc/Y/La, Ti/Zr/Hf, V/Nb/Ta) phases and related electronic configurations of the early μ d ($\mu = 3, 4, 5$) transition metals according to Equation 1. The most stable phases are marked in bold.

Phase	Formation energy ΔE_f (eV/f.u.) and related electronic configurations of T								
	Al ₃ Sc (3d ¹ 4s ²)	Al ₃ Ti (3d ² 4s ²)	Al ₃ V (3d ³ 4s ²)	Al ₃ Y (4d ¹ 5s ²)	Al ₃ Zr (4d ² 5s ²)	Al ₃ Nb (4d ³ 5s ²)	Al ₃ La (5d ¹ 6s ²)	Al ₃ Hf (5d ² 6s ²)	Al ₃ Ta (5d ² 6s ²)
L1 ₂	0.00	0.00	0.00	0.00	0.00	0.00	0.00	0.00	0.00
D0 ₂₂	0.36	-0.11	-0.54	0.51	0.00	-0.66	0.59	-0.08	-0.67
D0 ₂₃	0.18	-0.13	-0.27	0.26	-0.10	-0.33	0.28	-0.11	-0.34

Formatted: Subscript

Formatted: Subscript

Formatted: Font: Not Bold

Formatted: Font: Italic

Formatted: Font: Italic

Formatted: Font: Not Bold

Table III shows clearly the relation between the preferred structure and electron count in the TAl_3 family. With increasing number of electrons, the preferred structure transits from $L1_2$ - for $T = Sc/Y/La$ (d^1 elements) to $D0_{23}$ for $T = Ti/Zr/Hf$ (d^2) and further to $D0_{22}$ for $T = V/Nb/Ta$ (d^3).

Formatted: Superscript

Si replacing Al in TAl_3 indicates increasing number of electrons in the system and corresponding, it may cause phase changes. This is exemplified by Si dissolving at the Al1 sites in $D0_{22}$ - $ScAl_3$ (Figure 2). The remarkable stabilization effect is Si dissolving in $D0_{22}$ - $TiAl_3$. As shown in Figure 3, a moderate content of dissolving Si causes transition from the $D0_{23}$ - $TiAl_3$ to $D0_{22}$ - $Ti(Al_{1-x}Si_x)_3$ ($x > 0.02$). For $D0_{22}$ - VAl_3 , Si dissolving has little stabilization effect, since it contains already the highest number of electrons for this family. Naturally such stabilization effect due to increasing number of electrons holds for the related TAl_3 with $T = Y/La, Zr/Hf$ and Nb/Ta .

Table III shows also notable energetic differences for the TAl_3 phases with different transition metals. For example, the energy difference between $D0_{22}$ - and $D0_{23}$ - $TiAl_3$ is about 0.02 eV/f.u. which is notably smaller than that for $ZrAl_3$ (0.10 eV/f.u.). Correspondingly, the minimal Si content for the stabilized $D0_{22}$ - $Ti(Al_{1-x}Si_x)_3$ is small ($x \sim 0.02$), whereas it will be larger for stabilizing the $D0_{22}$ - $Zr(Al_{1-x}Si_x)_3$ over the $D0_{23}$ - $ZrAl_3$. Moreover, replacing Al by an element with less valence electrons, such as alkaline earth or noble metal elements reduces the electrons in the system, which may change the energetic hierarchy and the phase relation in the TAl_3 compounds in a reverse way. Effects of impurity solution in the TAl_3 compounds listed in Table III and for $T =$ e.g. Cr/Mo/W (d^4) elements, deserve further investigation.

Formatted: Font: Italic

Formatted: Subscript

Formatted: Superscript

4. Conclusions

First-principles density-function theory calculations for Si solutions on the $L1_2$ -, $D0_{22}$ - and $D0_{23}$ - Al_3T ($T = Sc, Ti$ and V) phases showed that Si prefer uniformly distribution in different layers of the same kind the same type of Al site. Si solution has a rich variety of effects on the stability of the Al_3T phases.

There is a link between the number of electrons in TAl_3 and the preferred structures: $L1_2$ - $ScAl_3$, $D0_{23}$ - $TiAl_3$ and $D0_{22}$ - VAl_3 . Si replacing Al increases the number of electrons in the systems, which may cause change of the corresponding preferred structures. This link also holds for the corresponding early 4d and 5d transition metal tri-aluminides.

Formatted: Font: Times New Roman, 10 pt

Formatted: Font: Times New Roman, 10 pt

Formatted: Font: Times New Roman, 10 pt, Subscript

Formatted: Font: Times New Roman, 10 pt

Formatted: Font: Times New Roman, 10 pt, Subscript

Formatted: Font: Times New Roman, 10 pt

Formatted: Font: Times New Roman, 10 pt, Subscript

Formatted: Font: Times New Roman, 10 pt

Formatted: Not Superscript/ Subscript

Formatted: Font: Times New Roman, 10 pt

Formatted: Font: Times New Roman, 10 pt

Formatted: Font: Times New Roman, 10 pt

Formatted: Font: Times New Roman, 10 pt

Formatted: Font: Times New Roman, 10 pt

Formatted: Font: Times New Roman, 10 pt

Si solution stabilizes $D0_{22}$ - Al_3Ti phase so that with the Si solutioned-partially dissolved phase it goes by the binary $D0_{23}$ - Al_3Ti . The partial substitution also induces extra freedom for the Si content at high temperatures. This explains the widely observed $D0_{22}$ -type particles in the commercial Al-based alloys which contains inevitably-variable degrees of Si. The most stable configuration has chemical formula, $D0_{22}$ - $(Al_{0.833}Si_{0.167})_3Ti$.

Si can be solutioned-dissolved at the Al1 and Al2 sites in and stabilize both $D0_{22}$ - and $D0_{23}$ - Al_3Sc phases. However, the Si stabilization is not enough to change their phase relations that the binary $L1_2$ - Al_3Sc structure keeps the ground state phase. The high energy cost indicates low Si doping in the cubic $L1_2$ - Al_3Sc crystals even at elevated temperatures.

Si solution is not favored in the Al_3V phases. Meanwhile, the energy cost for Si solution in the $D0_{22}$ -phase is moderate. Therefore, configurational entropy contribution enables moderate Si solution in $D0_{22}$ - Al_3V at elevated temperatures.

Crystallographically, Si solution reduces the lattice parameters in an almost linear way. This agrees with the rich variation of the lattice parameters for the $D0_{22}$ - $(Al,Si)_3Ti$ phase observed in the manufactured Al alloys.

The electronic structure calculations showed that strong bonding between Si and the transition metals. The Fermi level falls in the DOS valleys for the highly stable $L1_2$ - Al_3Sc , $D0_{22}$ - $(Al_{0.833}Si_{0.167})_3Ti$ and Si moderately doped $D0_{22}$ - $(Al_{1-x}Si_x)_3V$ (e. g. $x \sim 0.04$) phases.

Acknowledgements

The authors thank Dr. Yun Wang (BCAST) for beneficent discussions. Financial support from EPSRC (UK) under grant number EP/V011804/1 and EP/S005102/1 is gratefully acknowledged.

Conflict of Interest

The authors declare that they have no conflict of interest.

References

- 1). J.-F. Nie, *Physical metallurgy of light alloys*, in: D.E. Laughlin, K. Hono (Eds.), *Physical Metallurgy*, fifth ed., Elsevier, Oxford (UK), 2014.
- 2). M. V. Glazoff, A. V. Khvan, V. S. Zolotarevsky, N. A. Belov and A. T. Dinsdale, *Casting aluminum alloys*, Butterworth-Heinemann (Elsevier), Kidlington (UK)/Cambridge (USA) 2019.
- 3). J. W. Arblaster, *Selected values of the crystallographic properties of elements*, ASM International, Materials Park, Ohio (USA), 2018.
- 4). J. L. Murray, *J. Phys.: Equilib. Diffus.* II 19, 380 (1998).
- 5). V. Raghavan, *J. Phys.: Equilib. Diffus.* 26, 171 (2005).
- 6). H. Okamoto, *J. Phys. Equilib. Diffus. JPEDAV* 33, 491 (2012).
- 7). S. K. Shaha, F. Czerwinski, W. Kasprzak, J. Friedman and D. K. Chen, *Metal. Mater. Trans. A* 47A, 2396 (2016).
- 8). M. Očko, E. Babić, R. Krsnik, E. Girt and B. Leontić, *J. Phys. F: Metal Phys.* 6, 703 (1976).
- 9). J. Røyset and N. Ryum, *Intern. Mater. Rev.* 50, 19 (2015).
- 10). D. N. Seidman, E. A. Marquis and D. C. Dunand, *Acta Mater.* 50, 4021 (2002).
- 11). S. Z. Anvari, F. Karimzadeh and M. H. Enayati, *Mater. Sci. Technol.* 34, 179 (2018).
- 12). Y. B. Wang, Z. Y. Huang, W. Q. Hu, L. P. Cai, C. Lei, Q. Yu and Y. D. Jiao, *Mater. Charac.* 178, 111298 (2021).
- 13). C. Booth-Morrison, D. C. Dunand and D. N. Seidman, *Acta Mater.* 59, 7029 (2011).
- 14). K. Yan, Z. W. Chen, Y. N. Zhao, C. C. Ren, W. J. Lu and A. W. Aldeen, *J. Alloys Compd.* 861, 158491 (2021).
- 15). M. F. Liu, C. S. Zhang, Z. J. Meng, G. Q. Zhao and L. Chen, *Composites Part B* 226B, 109331 (2021).
- 16). Y. Meng, Y. Yang, C. Li, L.-G. Cao, Z.-H. Zhao, Q.-F. Zhu and J.-Z. Cui, *Trans. Nonferrous Met. Soc. China* 32, 2110 (2022).
- 17). G. M. A. Mahran and A.-N. M. Omran, *Mater. Sci. (Medziagotyra)* 28, 41 (2022).
- 18). M. Easton and D. StJohn, *Metal. Mater. Trans. A* 30A, 1613 (1999).
- 19). G. S. Vinod Kumar, B. S. Murty and M. Chakraborty, *J. Mater. Sci.* 45, 2921 (2010).
- 20). P. Schumacher, A. L. Greer, J. Worth, P. V. Evans, M. A. Kearns, P. Fisher and A. H. Green, *Mater. Sci. Techn.* 14, 394 (1998).
- 21). Z. Fan, Y. Wang, Y. Zhang, T. Qin, X. R. Zhou, G. E. Thompson, T. Pennycook and T. Hashimoto, *Acta Mater.* 84, 292 (2015).
- 22). J. H. Li, F. S. Hage, Q. M. Ramasse and P. Schumacher, *Acta Mater.* 206, 116652 (2021).
- 23). F. Foadian, M. Soltanieh, M. Adeli and M. Etmianbakhsh, *Metall. Mat. Trans. B* 47B, 2931 (2016).
- 24). J. Atherton, *Int. J. Life Cycle Assess.* 12, 59 (2007).
- 25). D. Raabe, D. Ponge, P. J. Uggowitzer, M. Roscher, M. Paolantonio, C. L. Liu, H. Antrekowitsch, E. Kozenschnik, D. Seidmann, B. Gault, F. De Geuser, A. Deschamps, C. Hutchinson, C. H. Liu, Z. M. Li, P. Prangnell, J. Robson, P. Shanthraj, S. Cakili, C. Sinclair and S. Pogatscher, *Prog. Mater. Sci.* 128, 100947 (2022).
- 26). R. W. G. Wyckoff, *Crystal Structures*, John Wiley, New York (USA), 1963.
- 27). C. M. Fang and Z. Fan, *Comp. Mater. Sci.* 153, 309 (2018).
- 28). X. Y. Zhang, Y. C. Huang, Y. Liu, and X. W. Ren, *Results in Physics* 19, 103378 (2020).
- 29). Z. Chen, P. Zhang, D. Chen, Y. Wu, M. L. Wang, N. H. Ma and H. W. Wang, *J. Appl. Phys.* 117, 085904 (2015).
- 30). C. Amador, J. J. Hoyt, B. C. Chakoumakos and D. de Fontaine, *Phys. Rev. Lett.* 74, 4955 (1995).
- 31). J. C. Schuster and M. Palm, *J. Phase Equilib. Diffus.* 27, 255 (2006).
- 32). J. L. Murray, *Binary Alloys Phase Diagrams*, in: T.G. Massalski (Ed.), ASM, Metals Park, Ohio (USA), 1986.
- 33). F. J. J. van Loo and G. D. Rieck, *Acta Metallurgica* 56, 61 (1965).
- 34). S. Srinivasan, P. B. Desch and R. B. Schwarz, *Scripta Metall. Mater.* 125, 2513 (1991).
- 35). M. H. Lee, J. Lee and Z.-H. Lee, *Scripta Metal.* 25, 517 (1991).

- 36). R.B. Schwartz, P.B. Desch, S. Srinivasan, *Static and Dynamics of Alloys Phase Transformation*, Plenum Press, New York (USA),1994.
- 37). C. M. Fang, Z. P. Que and Z. Fan, *J. Solid State Chem.* 299, 122199 (2021).
- 38). Z. Li, C. L. Liao, X. M. Wang, Y. Wu, M. X. Zhao, Z. H. Long and F. C. Yin, [JPEDAV-J. Phase Equilib. Diffus.](#) 35, 564 (2014).
- 39). J.-R. Castillo-Sánchez, G. Salloum-Abou-Jaoude, A. E. Gheribi, P. Lafaye, K. Oishi, J.-P. Masse, E. Bousser, G. L'Espérance and J.-P. Harvey, *Acta Mater.* 262, 119455 (2023).
- 40). R. Boulechfar, D. Sayad, Y. Khenioui, H. Meradji, S. Ghemid, R. Kenata, S. Bin-Omran, A. Bouhemadou and S. Goumri-Said, *Eur. Phys. J. B* 97B, 1(2024).
- 41). Z. Ahmad, *J. Metals* 55, 35 (2003).
- 42). Y. Harada and D. C. Dunand, *Mater. Sci. Engin. A* 329-331A, 686 (2002).
- 43). J. Dumre, S. K. Kairy, E. Anber, T. Langan, M. L. Taheri, T. Dorin and N. Birbilis, *J. Alloys Compd.* 861, 158511 (2021).
- 44). Q. Yao, *Adv. Mater. Res.* 284-286, 1987(2011).
- 45). G. Kresse and J. Furthmüller, *Comp. Mater. Sci.* 6, 15 (1996).
- 46). J. P. Perdew, K. Burke, and M. Ernzerhof, *Phys. Rev. Lett.* 77, 3865 (1996).
- 47). P. E. Blöchl, Projector augmented-wave method, *Phys. Rev. B.* 50B, 17953 (1994).
- 48). C. M. Fang, Z. P. Que, A. Dinsdale and Z. Fan, *Intermetallics* 126, 106939 (2020).
- 49). C. M. Fang, M. A. van Huis, M. H. F. Sluiter, and H. W. Zandbergen, *Acta Mater.* 58, 2968 (2010).
- 50). H. J. Monkhorst and J. D. Pack, *Phys. Rev. B.* 13B, 5188 (1976).
- 51). N. Blake and M. A. Hopkins, *J. Mater. Sci.* 20, 2861 (1985).
- 52). M. Zedalis and M. E. Fine, *Script Metall.* 17, 1247 (1983).
- 53). S. Guo and C. T. Liu, *Prog. Nat. Sci: Mater. Intern.* 21, 433 (2011).
- 54). Y.-H. Duan, B. Huang, Y. Sun, M.-J. Peng and S.-G. Zhou, *Chin. Phys. Lett.* 31, 088101 (2014).
- 55). E. C. Stoner, *Proc. Royal soc. A* 165A, 372 (1938).
- [56\). W.-S. Chang and B. C. Muddle, *Metals and Mater.* 3, 1 \(1997\).](#)

Formatted: Font: Times New Roman, 10 pt